Experimental and numerical modelling of buried pipelines crossing reverse faults

Hasan Emre Demirci [1], Subhamoy Bhattacharya [2], Dimitrios Karamitros[3], Nicholas Alexander[4]

[1]PhD Candidate, Civil and Environmental Engineering, University of Surrey, Guildford, GU2 7XH, United Kingdom, h.demirci@surrey.ac.uk
[2]Professor and Chair in Geomechanics, Civil and Environmental Engineering, University of Surrey, Guildford, GU2 7XH, United Kingdom, s.bhattacharya@surrey.ac.uk
[3]Lecturer in Geotechnical Engineering, Department of Civil Engineering, University of Bristol, Bristol, BS8 1TH, United Kingdom, d.karamitros@bristol.ac.uk
[4]Senior Lecturer in Structural Engineering, Deparment of Civil Engineering, University of Bristol, Bristol, BS8 1TH, United Kingdom, Nick.alexander@bristol.ac.uk

Corresponding Author:
Subhamoy Bhattacharya
Professor & Chair in Geomechanics
University of Surrey Guildford, United Kingdom, GU2 7XH
S.Bhattacharya@surrey.ac.uk
Phone number: 01483689534

Abstract: Fault rupture is one of the main hazards for continuous buried pipelines and the problem is often investigated experimentally and numerically. While experimental data exists for pipeline crossing strike-slip and normal fault, limited experimental work is available for pipeline crossing reverse faults. This paper presents results from a series of tests investigating the behaviour of continuous buried pipeline subjected to reverse fault motion. A new experimental setup for physical modelling of pipeline crossing reverse fault is developed and described. Scaling laws and non-dimensional groups are derived and subsequently used to analyse the test results. Three-dimensional Finite Element (3D FE) analysis is also carried out using ABAQUS to investigate the pipeline response to reverse faults and to simulate the experiments. Finally, practical implications of the study are discussed.

Keywords: 1-g scale models, buried pipeline, reverse faulting, permanent ground deformation, earthquake

1. Introduction

Earthquake induced permanent ground deformation (PGD) can severely affect the behaviour of buried pipelines. Ground fault rupture, which causes PGD, is one of the major seismic hazards for lifeline facilities such as gas and water supply pipelines. Past earthquakes; (see for example, 1999 Kocaeli and 1999 Duzce, 1999 Chi Chi, 2008 Wenchuan, 2009 Italy, 2010 Chile) showed that pipelines are extremely vulnerable to earthquake induced PGDs. The effects of pipeline failures on world industry, economy and society can be very devastating. For example, extensive damage occurred on Trans-Ecuadorian pipeline during 1987 Ecuador Earthquake and the economics loss is approximately $850 million in lost sales and reconstruction (National Research Council, 1991). During the 1906 San Francisco earthquake, the water mains broke leaving the fire department with limited water resources to fight fires (O'Rourke, 2010). Thus, the evaluation of pipeline performance during and after earthquakes requires particular attention in order to mitigate effects of PGDs on buried pipelines. Table A-1 in Appendix details 13 pipeline failure case records from the fault crossing zones collated from 10 different earthquakes.

It is of interest to draw some broad conclusions from these case records:

(1) The failure type can be of following types: beam buckling (similar to Euler buckling of columns), local buckling (instability of the shell) (see in Figure 1), tensile failure (yielding and fracture) and joint failure.

(2) Steel pipelines are commonly used in the field to transport water, oil and gas. Being long and slender, they are relatively weak under compressive loading. In this context, it is important to highlight that pipelines passing through reverse faults and some type strike-slip faults will induce compressive load on pipelines.

(3) 18^{th} Column of the Table A-1 estimates the normalised fault displacement denoted by (δ/D) where δ is the observed fault displacement and D is the pipe

diameter. In most cases, the ground moved past the pipe. Following Bouzid et al. (2013), average shear strain in the soil around the mobilized deformation zone can be estimated as 2.6×(y/D) where y is the pipe displacement. It may therefore be inferred that the soil-pipe interaction in a fault crossing zone is large strain problem and Large Deformation Finite Element (LDFE) is necessary.

1.1. A brief review of literature

A large body of research including analytical, numerical and experimental have been conducted in the past four decades to study pipeline performance during earthquakes. Newmark and Hall (1975) developed simplified analytical methods for the pipeline crossing faults which is primarily subjected to tensile strain. Kennedy et al. (1977) extended the work of Newmark and Hall (1975) by taking into account lateral interaction effects at the pipe-soil interface and large axial strain effects on the bending stiffness of the pipe. Wang and Yeh (1985) proposed modifications to closed-form analytical model by representing the pipeline-soil system using concept of the theory of beams on elastic foundations. The pipeline was partitioned into four segments where two segments are in high deformation zone and other two segments are in small deformation zone. Beams on elastic foundation approach was used to analyse the segments in small deformation zone while the segments in high deformation zone were assumed to deform as circular arcs. Takada et al. (2001) proposed a new simplified semi-analytical method to obtain maximum pipe strain in steel pipelines crossing faults considering nonlinearity of material and deformation of pipe cross-section. They proposed simplified formulations to calculate maximum tensile and compressive pipe strains by using pipe bending angle. Existing analytical methodologies were refined by Karamitros et al. (2007) to achieve a wider range of applications. The equations proposed by Kennedy et al. (1977) were used to take into account the effects of axial tension on the pipeline curvature together with Wang and

Yeh model (1985). The nonlinear behaviour of pipeline material was taken into account by carrying out a series of equivalent linear calculation loops, where the secant Young's modulus of the pipe material is readjusted on each loop. Trifonov and Cherniy (2010) developed an analytical methodology proposed by Karamitros et al. (2007) to analyse the response of pipelines crossing normal faults. They considered no symmetry condition about the fault-pipeline intersection to be able to analyse different types of fault mechanisms. Karamitros et al. (2011) extended the earlier analytical methodology of Karamitros et al. (2007) for the stress-strain analysis of buried steel pipelines crossing strike-slip faults to normal faults. Trifonov and Cherniy (2012) presented an analytical model for stress-strain analysis of buried steel pipelines crossing active faults, taking into account the influence of operational loads such as internal pressure and temperature variation on the basis of plane strain plasticity theory.

Finite Element Method is one of the useful tools to explore the response of pipeline subjected to PGD, taking into account the nonlinearity of soil and pipe and the interaction between soil and pipe. Finite element method has been recently used by several researchers for the verification and refinement of analytical methods, the evaluation of factors influencing pipe response under different types of PGD, the assessment of pipeline performance with respect to performance criteria such as local buckling, ovalization and tensile rupture (Lim et al., 2001; Takada et al., 2001; O'Rourke et al., 2003; Sakanoue and Yoshizaki, 2004; Karamitros et al., 2007; Xie et al., 2011; Vazouras et al., 2010, 2012, 2015; Trifonov, 2015, Zhang et al., 2016). In a recent study, Liu et al. (2016) modelled the pipeline response to reverse faulting using FE software ABAQUS. In the study, the pipe was modelled as shell elements and pipe-soil interaction was modelled as non-linear soil springs. In the work, the effects of yield strength and strain hardening parameters is investigated from the point of view of buckling response. A review of the Finite Element (FE) models in the literature indicates that various types of models including beam, shell, hybrid (beam+shell), soil continuum-shell model are utilized in order to

simulate pipeline response to PGD. However, the verification of FE analysis results is essential to obtain reliable outcomes. Due to lack of verified case histories, there is a need to perform scaled model tests not only to identify mechanisms but also for verification and calibration of analytical and numerical methodologies.

Palmer et al. (2006) described the large-scale testing facility at Cornell University and the working principle behind them. O'Rourke and Bonneau (2007) performed large scale tests in order to evaluate the effects of ground rupture on HDPE (High Density Poly Ethylene) pipelines and the performance of steel gas distribution pipelines with 90^0 elbows. Lin et al. (2012) performed small-scale tests to analyse the performance of buried pipelines under strike-slip faults. Centrifuge based approach was first proposed by O'Rourke et al. (2003, 2005) to model ground faulting effects on buried pipelines. Ha et al. (2008), Abdoun et al. (2009), Ha et al. (2010) and Xie et al. (2011) performed several centrifuge tests to investigate response of buried pipeline to ground faulting. The centrifuge based tests were performed for the verification of numerical and analytical methodologies, the evaluation of parameters affecting pipeline response to faulting and the assessment of soil-pipe interaction (soil spring model in ASCE 1984). As viewed in the literature, a significant number of studies have been performed on the pipe response to strike-slip faulting. However, there are limited experimental works on pipeline performance under reverse fault motion and is therefore the focus of this study.

1.2. Aims & Scope of the Work

The aims and scope of the paper are as follows:

1) To describe a new experiment setup developed to study the effects of reverse faulting on buried continuous pipeline.
2) To present the test results using non-dimensional groups so that a framework of understanding can be developed.

3) To compare three-dimensional (3D) FE analysis results with experimental results in order to verify/validate 3D FE model.

2. Experimental Modelling

Buried pipelines subjected to reverse faulting primarily undergo compression combined with bending and shear. The combination of bending and compression strains causes different types of pipeline failure modes such as local buckling and beam buckling (Figure 1). Particularly, local (shell) buckling failure mode are very destructive for pipeline integrity. Therefore, soil-pipeline interaction under reverse faults should be investigated to increase earthquake resilience of pipelines crossing reverse faults.

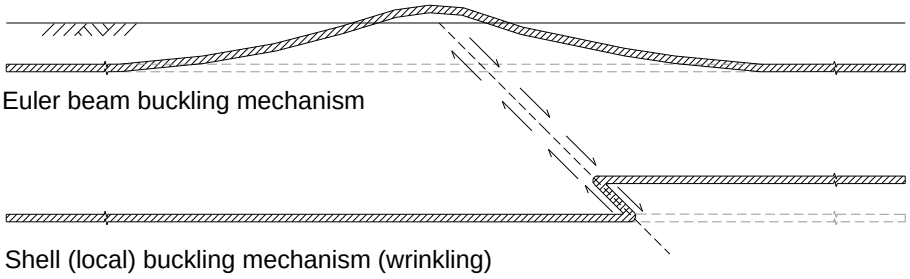

Figure 1. Illustration of the two distinct buckling failure mechanisms

Pipelines crossing active faults can be modelled as a beam on elastic foundation, see Figure 2. Steel pipelines in the field have small cross-sectional dimensions compared to distances along its axis i.e. distance between support points. Therefore, they can be considered as slender beams and Euler-Bernoulli beam approach can therefore be used to model these pipelines. The soil surrounding pipelines is also assumed to be uniform. The governing equation of the problem is very similar to the laterally loaded beam on elastic uniform support. Figure B-2 in the Appendix shows a free body diagram of the segment of pipeline crossing strike-slip faults. The governing equation of laterally loaded beam on elastic uniform support is derived from the free body diagram (explained in the Appendix B) and given as follow:

$$EI\frac{d^4w}{dx^4}+\left(P-\int_0^x f(x)dx\right)\frac{dw^2}{dx^2}-f(x)\frac{dw}{dx}+k\cdot w=F \qquad (1)$$

where

EI = Bending stiffness of the pipe

w = Transverse deflection of the pipe

$f(x)$= The friction per length (T_u)

k = Soil stiffness (in compression)

P = External axial load on pile/beam head (for pipelines crossing active faults, P=0)

F = External loads which may be present at the surface level, e.g. roadways

It is convenient to express equation of motion (1) in terms of non-dimensional parameters by elementary re-arrangements as:

$$\frac{\mathrm{d}^4\mathrm{W}(\xi)}{\mathrm{d}\xi^4}+\left(\frac{\mathrm{P_x D^2}}{\mathrm{EI}}\right)\frac{\mathrm{d}^2\mathrm{W}(\xi)}{\mathrm{d}\xi^2}-\left(\frac{\mathrm{f(x)D^3}}{\mathrm{EI}}\right)\frac{\mathrm{dW}(\xi)}{\mathrm{d}\xi}+\left(\frac{kD^4}{EI}\right)\mathrm{W}(\xi)=F \qquad (2)$$

where P_x is axial force in the pipeline at location x and formulated as $P-\int_0^x f(x)\partial x$ and D is pipe diameter and ξ is non-dimensional length parameter (x/D).

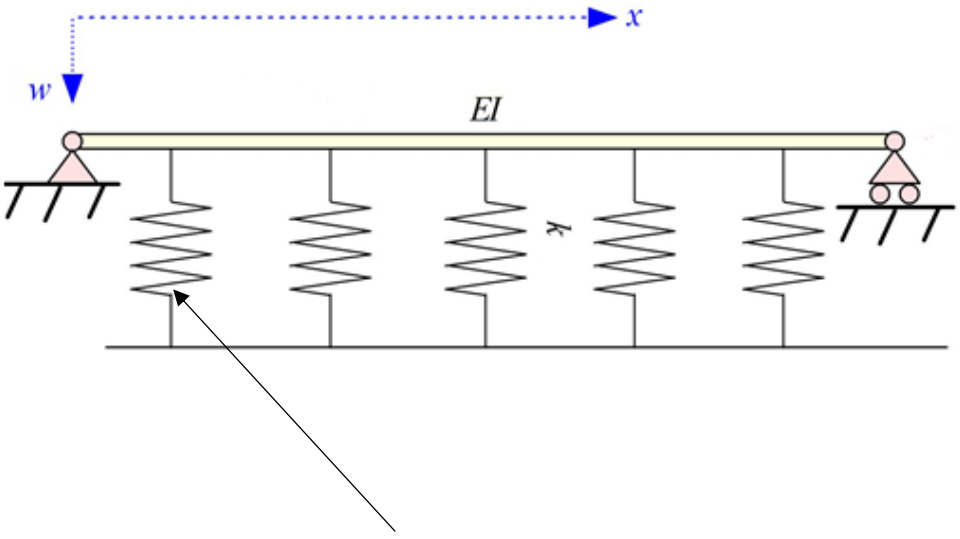

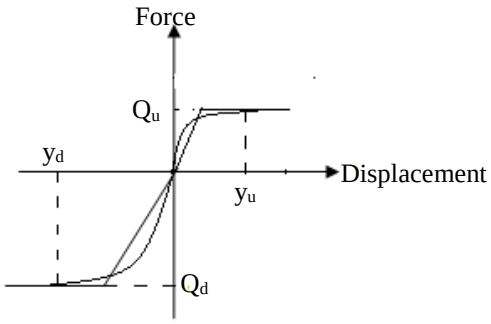

Figure 2. Pinned-pinned beam resting on uniform elastic support

Each of the non-dimensional groups in the parenthesis has a physical meaning. For example, $(P_x D^2 / EI)$ represents the non-dimensional axial force, $(f(x)D^3 / EI)$ is non-dimensional soil-pipe friction and $(k(x)D^4 / EI)$ is relative soil-pipe stiffness. The next section derives the scaling laws and similitude relations for the pipeline crossing reverse fault.

2.1. Similitude relationships / Scaling laws

Modelling the behaviour of pipelines subjected to faulting is very complex and involves various interactions. The main interaction occurs between soil and pipeline due to the relative displacement between them. This relative movement causes the pipe to be loaded both vertically and axially. Consequently, bending and axial strains arise in the pipe due to the interaction between soil and pipe. The rules of similarity between the model and the prototype that need to be maintained are:

(1) Relative soil-pipe stiffness (kD^4/EI): The stiffness of the soil relative to the pipe needs to be preserved in the model so that the pipe interacts similarly with the soil as in the prototype. Pipeline flexibility affects soil-structure interaction as a result influences pipeline response to faulting.

$$\left(\frac{kD^4}{EI}\right)_{model} \cong \left(\frac{kD^4}{EI}\right)_{field} \tag{3}$$

Figure 3 shows normalised stress-strain curves of 3 different pipe materials: API-X65 which is commonly used for practical applications (i.e. prototype) and the remaining two (aluminium alloy and brass) are model pipe candidates. All the three pipeline materials have similar bi-linear behaviour in the sense that linear elastic behaviour followed by a different post-yield behaviour. The non-dimensional parameter given by Equation 3 is essentially relative soil-pipe stiffness and dictates the deformation behaviour (flexible or rigid body). The different pipe material can be incorporated in Equation 3 through the Young's Modulus (E) parameter. If the model test results obtained using one pipe material is to be scaled to predict the prototype behaviour of pipe of another material, the inelastic post-yield response of the stress-strain curve also need to be considered. In such scenarios, it is often useful to incorporate the mechanism understood from scaled model tests and predict the prototype through numerical modelling whereby customised stress-strain behaviour of the pipeline material can be implemented.

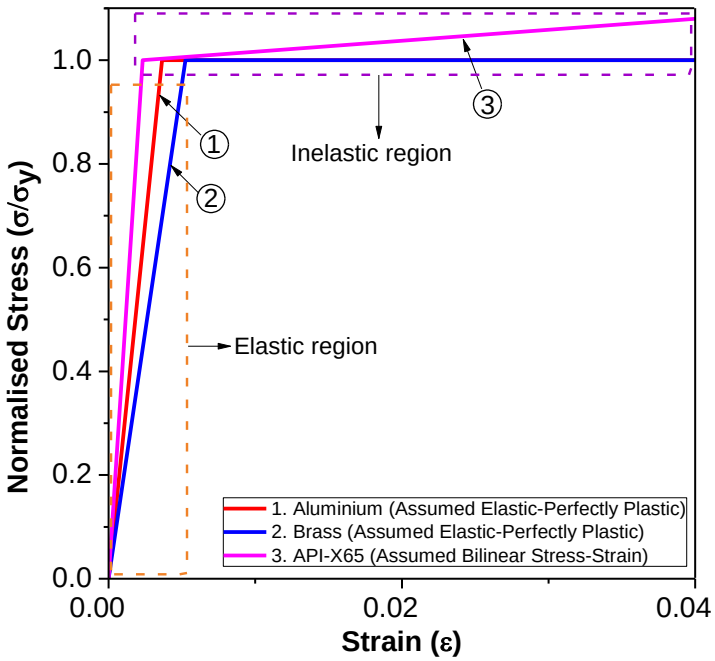

Figure 3. Normalised Stress-Strain curves for Aluminium, Brass and API-X65 Steel

(2) *Normalised Soil-Pipe Friction ($f(x)D^3/EI$):* Soil-pipe friction force along the pipeline axis occurs due to relative movement of soil and pipe in the axial direction. This force depends on mean confining stress (p') on the pipeline, pipe outer surface (k), adhesion factor (α) and soil parameters: cohesion (c) and internal friction angle (φ).

$$\left(\frac{\mathrm{f(x)D^3}}{\mathrm{EI}}\right)_{model} \cong \left(\frac{\mathrm{f(x)D^3}}{\mathrm{EI}}\right)_{field} \tag{4}$$

The axial soil pipe friction force (f(x)) can be calculated based on Equation 5:

$$f(x) = \pi D\alpha c + \pi DH\gamma\left(\frac{1+K_0}{2}\right)tank\emptyset \tag{5}$$

where H is burial depth of the pipe, γ is unit weight of the soil and K_0 is coefficient of lateral pressure at rest.

(3) Geometric similarity: The dimensions of the small-scale model need to be selected in such a way that similar pipeline response will be observed in model and prototype. It is expected that beam and local buckling failure modes govern the pipeline response to reverse faults. Thick walled pipelines (small pipe diameter to wall thickness ratio denoted by D/t) buried at shallow depths (small burial depth to pipe diameter denoted by H/D) experience beam buckling failure whilst thin walled pipelines (large D/t ratio) buried at deeper depths (large H/D ratio) experience local buckling failure. Therefore, D/t and H/D ratios of the model should be kept consistent with the values for the prototype.

$$\left(\frac{D}{t}\right)_{model} \cong \left(\frac{D}{t}\right)_{field} \tag{6}$$

$$\left(\frac{H}{D}\right)_{model} \cong \left(\frac{H}{D}\right)_{field} \tag{7}$$

(4) *Scaling of soil:* Grain size effects on soil-pipe interaction are a significant issue in scaled tests. The similitude of the ratio between the pipe diameter (D) and the average soil grain size (d_{50}) is determined by applying the result of the investigation of Bolton et al. (1993) on the relationship between cone diameter and d_{50}. In addition, the smallest ratio of pipe diameter to average soil grain size (D/d_{50}) can be chosen according to the criterion of $D/d_{50} \geq 48$ recommended by the International Technical Committee TC2 (2005) based on centrifuge test data from Ovesen (1981) and Dickin and Leuoy (1983). Red Hill 110 dry silica sand is chosen for experimental investigation by considering suitable ratio between D and d_{50}. A shear box test based on the methodology of BS 1377 is performed to determine the friction angle of the soil. The engineering properties for Red Hill 110 dry sand is illustrated in Table 1.

$$\left(\frac{D}{d_{50}}\right) \geq 48 \tag{8}$$

Table 1. Engineering properties for Red Hill 110 dry sand

d_{10} Grain Size	85μm
d_{50} Grain Size	144μm
d_{90} Grain Size	210 μm
Angle of Friction, $\emptyset'_{critical}$	34° (as measured)
Specific Gravity, G	2.65
Maximum Void Ratio, e_{max}	1.04
Minimum Void Ratio, e_{min}	0.55

(5) Scaling of fault movement: The fault displacement (δ) will be assessed by the ratio of fault displacement to the pipe diameter (δ/D), in order that the fault movement in the experimental model is of a comparable magnitude to real fault movements. Fault displacements vary considerably in the field with displacements of up to 8m observed in the 1999 Chi-Chi Taiwan earthquake (EERI, 1999). For a typical pipeline diameter

400mm, the relative fault displacement (δ/D) tests would be as large as 20. The large displacement tests will therefore be limited to a value of δ/D to 20.

$$\left(\frac{\delta}{D}\right)_{model} \cong \left(\frac{\delta}{D}\right)_{field} \tag{9}$$

The scaling of fault offset rate is not considered in this study. However, the fault movement will be applied at an approximately constant rate throughout the tests to enable comparison of the data.

(6) Scaling of Anchorage: A sufficient length of pipe on either side of the fault is necessary to achieve anchorage in order to simulate field conditions. The non-dimensional group used to scale anchorage length is the ratio of anchor length of pipe to pipe diameter (L_a/D). Literature review indicates that required anchorage length is a function of fault displacement, pipe diameter, and burial depth (Kennedy et al., 1977) and that even for small fault displacement several hundreds of pipe diameters of length are needed for sufficient anchorage. Therefore, the experimental work aims to maximise the length of pipeline either side of the fault.

$$\left(\frac{L_a}{D}\right)_{model} \cong \left(\frac{L}{D}\right)_{model} \tag{10}$$

where $L_a = (\sigma_y \cdot A)/T_u$, ($\sigma_y$ is yield stress of pipe material, A is cross-section area of pipe and T_u is limit friction due to slippage of the pipeline relative to the surrounding soil), L is pipe length between fault intersection point and end connection (see Figure 7).

The non-dimensional groups derived are summarised in Table 2 and the typical values of these groups from the field case records are given in Table 3. It is important to state that the scaling laws derived are strictly applicable in the elastic range.

2.2 Other issues related to 1-g scale model tests

The soil behaviour is stress-dependent and nonlinear. Soils may experience dilative behaviour at low stress level whereas contractive behaviour of loose to medium sand is observed under high normal stress. The stress level in 1-g small scale models is much lower than its equivalent prototype, leading to higher friction angle of soil. Many researchers (Kelly et al., 2006; Leblanc et al., 2010, Bhattacharya et al., 2012)), dealt with this issue by pouring the sand at lower relative density. Bolton (1986) proposed an equation based on his stress-dilatancy work showing the variation of the peak friction angle (ϕ') with mean effective isotropic stress (p').

$$\phi' = \phi_{cv} + 3\left[R_D\left(9.9 - \ln p'\right) - 1\right] \tag{11}$$

where R_D is relative density of the sand and ϕ_{cv} is critical state angle of friction of the sand.

Table 2. Scaling laws for studying soil-pipe interaction under faulting

Name of the non-dimensional group	**Physical Meaning**	**Remarks**
(kD^4/EI)	Flexibility of the pipeline so as to have similar soil-structure interaction	Small (kD^4/EI): rigid pipe behaviour Large (kD^4/EI): flexible pipe behaviour
(D/t)	Slenderness of the pipeline (affects pipeline failure mode)	Large (D/t): shell buckling failure mode Small (D/t): beam buckling failure mode
(H/D)	Non-dimensional burial depth (affects soil failure type)	Small (H/D): wedge type of soil failure Large (H/D): soil flow around the pipe
(L_a/D)	Non-dimensional anchor length	Providing anchor length results in no boundary effects at both end sides of the pipe ($L_a=\sigma_y A/t_u$)
(d_{50}/D)	Non-dimensional average soil grain size	Grain size effects on soil-pipe interaction
(δ/D)	Non-dimensional fault displacement (strain field in the soil around the pipeline)	Similar strain field will control soil-pipe interaction

In the experimental study, Red Hill 110 dry silica sand is poured at low relative density to ensure that the peak friction angle is close to the values in the field. 1g small scale models have another issue related to shear modulus (G) of soils. The shear modulus of a soil increases with

increasing mean confining stress. The stress level in the small-scale models is much lower than in the field. The shear modulus of a soil (G) is dependent on effective stress and can be expressed by Equation 12.

$$G \propto p'^{n} \tag{12}$$

The value of n ranges between 0.435 and 0.765 for sandy soils (Wroth et al., 1979) but the value of n is generally taken as 0.5 for sandy soils. A value of 1 is generally used for clayey soils. The issue of stiffness is taken care by non-dimensional groups.

Table 3. Values of non-dimensional groups for field and model pipelines

Non-dimensional group	**Field (prototype) values (Range)**	**Model values (Range)**
kD^4/EI	0.00022-0.0083	0.00023-0.0003
D/t	9.27-122	11.11
H/D	1-50	5-40
δ/D	1.36-21.17	1-20

2.3. Experimental Setup

Figure 4 shows the experimental test setup used along with schematic explanation of the working principle. The box has 2m length, 0.4m width and 0.75m depth. Force is applied to moveable back piece by scissor jack connected with hydraulic jack. Since moveable back piece moves in lateral direction, moveable hanging wall moves in both lateral and upward direction. PTFE (Poly Tetra Fluoro Ethylene) material is attached to all timber sliding faces to minimise the surface friction between the surfaces of timber components. The test setup represents fault

crossing angle=90° and fault dip angle=45°. The scaled 1-g model allows for a maximum vertical displacement of 150mm. Figure 4c shows observed shear bands after application of displacement to the hanging wall in both horizontal and vertical planes. As mentioned in Section 2.2, the confining pressures in 1g small-scale models are extremely low compared to its equivalent prototype. It is expected that granular materials like Red Hill 110 dry sand will exhibit strongly dilatant behaviour under low confining pressures. Granular soils experience strongly volume change under shear deformation at very low confining pressures. Therefore, the stress levels can change the patterns of rupture propagation through the sand deposit. The other parameters influencing patterns of rupture propagation are the thickness of sand deposit, ductility or fragility of sand deposit, grain size (Lee et al., 2004; Stone and Wood, 1992, Johansson and Konagai, 2005). The boundary conditions and initial stress conditions are important factors on shear band development. In experiments, rigid boundaries are commonly used and these rigid boundaries should be placed far away from the large shearing region (Johansson and Konagai, 2005). Otherwise, the boundaries may influence shear band development and the development of shear bands will be function of the length of the set-up used.

The main purpose of the experimental testing are as follows:

(1) To understand the behaviour of buried continuous pipeline subjected to reverse faulting.
(2) To study the effect of burial depth on buried continuous pipeline subjected to reverse fault motion.
(3) To evaluate relative soil-pipe stiffness (kD^4/EI) effects on the pipe response to reverse faults.

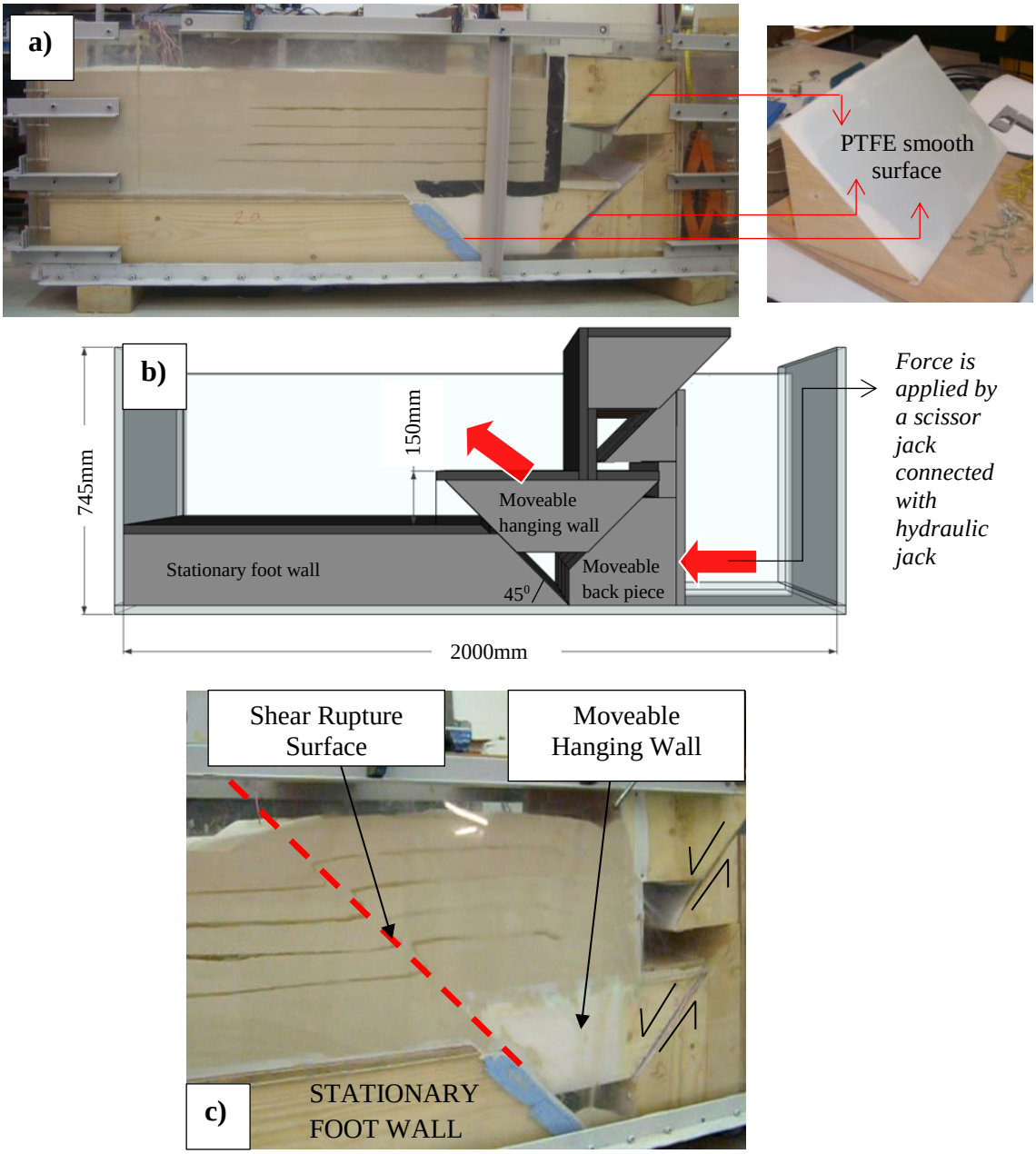

Figure 4. a)1-g physical model of buried pipeline subjected to reverse fault, b) working principle of 1-g scaled model, c) observed shear bands after application of displacement in both horizontal and vertical planes

Two different pipe materials are used in the experiments in order to investigate the effects of kD^4/EI on the behaviour of pipelines crossing reverse faults. The pipe materials used in the experiments are aluminium alloy and brass alloy. The engineering properties of pipe materials are obtained from tensile loading tests based on methodology of ASTM B557M and three point bending tests based on the methodology of ASTM E855-08 (Figure 5). The pipe material

properties and dimensions are illustrated in Table 4 and the results of tensile loading tests for aluminium and brass tube are demonstrated in Figure 6.

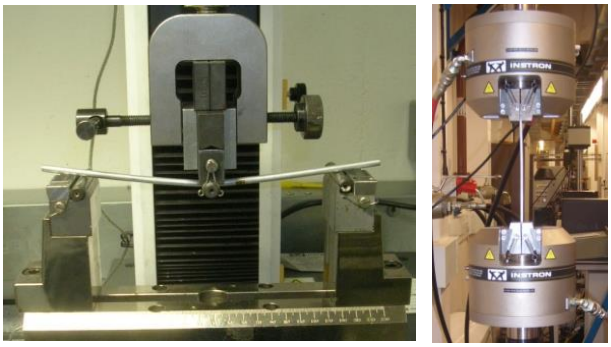

Figure 5. Photographs of three point bending test (left) and tensile loading test (right)

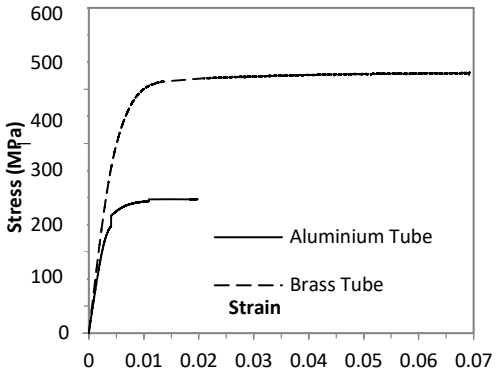

Figure 6. Stress-strain relationship obtained from tensile loading tests

Table 4. Pipe material properties and dimensions

	Aluminium Alloy	**Brass Alloy**
Young's Modulus, E	66 GPa	84GPa
Yield Stress, σ_y	240MPa	440MPa
Outer Diameter, D	5mm	5mm
Wall Thickness, t	0.45mm	0.45mm

Five pairs of quarter bridge strain gauges at opposing sides of the pipe are used to measure the strain in the pipeline. This configuration of strain gauges permitted for the calculation of axial strain and bending strain in the pipeline from the strain gauge data. Bending strains are calculated as one-half the difference between the longitudinal strains at opposite sides of pipe (Equation 13). The signal from the strain gauges is amplified and recorded on the computer by using A/D channels and D-Space Control Desk. The raw output obtained from the gauges is a voltage that is converted to strain using Equation 14.

$$\varepsilon_b = \left(\frac{\varepsilon_1 - \varepsilon_2}{2} \right) \tag{13}$$

$$\varepsilon = \left(\frac{4V_{comp.}}{F \cdot V_s \cdot G} \right) \tag{14}$$

where $V_{comp.}$= Voltage displayed on computer, F=strain gauge factor, V_s=excitation voltage, G=strain gauge amplification factor.

3. Experimental Results

In the scope of experimental works, 20 tests have been performed and these tests have been grouped into three distinct series: exploratory, large displacement and small displacement tests. The purpose of exploratory tests is to determine the suitability of various boundary conditions in modelling the field conditions. Both large displacement (LD) tests and small displacement (SD) tests have been performed to evaluate the plastic and elastic pipeline response to reverse faulting. The fault and pipe characteristics observed during past earthquakes are given in Table 5. It is seen that the ratio of fault displacement to pipe diameter ranges between 1.4 and 5. Hence, the special focus is given to the small displacement tests by performing 17 SD tests. The bending and axial strains developed in the pipeline are measured by all the tests. The axial strains were not symmetric at two sides of fault due to an artificial effect of the non-symmetric boundary conditions, which is not realistic. Nevertheless, the corresponding strains were actually very small compared to bending strains and they were neglected. The maximum axial strains were around 0.015 of yield strain. This is a limitation of the experiment and that in reality axial strains would also develop along the pipeline.

There are five pairs of strain gauges on the pipeline and therefore, bending strains can be calculated for only five different locations on the pipeline. Polynomial fit technique is used to predict the distribution of bending strains along the pipeline.

Table 5. Fault and pipe characteristics during past earthquakes

	Fault Characteristics		Pipe Characteristics			
Earthquake	**Slip Type**	**Max. Displacement (δ)**	**Nature of Content**	**Pipe Diameter**	**δ/D**	**Reference**
1954 Kern County	Left Lateral Reverse	1300	Gas	864	1.5	Denis, R., 2001
1971 San Fernando	Thrust	2000	Gas	400	5	SCGC, 1973
1999 Turkey	Right Lateral Strike Slip	3000	Water	2200	1.4	Ha et al.,2008
1999 Turkey	Right Lateral Strike Slip	3000	Water	700	4.3	Earthquake Spectra, 2000

3.1. Exploratory Tests

Exploratory tests are performed to determine the most appropriate boundary condition that replicate the field conditions accurately. Three particular boundary conditions used in exploratory tests are illustrated in Figure 7. The fixed boundary condition is created by inserting the pipeline into a slot in the moving or stationary wall respectively, thus providing bearing in the axial plane and fixing the position in the vertical and lateral planes. The exploratory tests are performed at the ratio of burial depth to pipe diameter (H/D) = 40, aiming to engage the critical failure mechanism of local buckling. The exploratory tests reveal insufficient anchorage as demonstrated by movement of the pipe from its original position in Exp-03 (Table 6). The summary of the exploratory tests where fault displacement continued up to 20-25D is shown in Table 6. The deformed shape for Exp-1 and Exp-2 is illustrated in Figure 8.

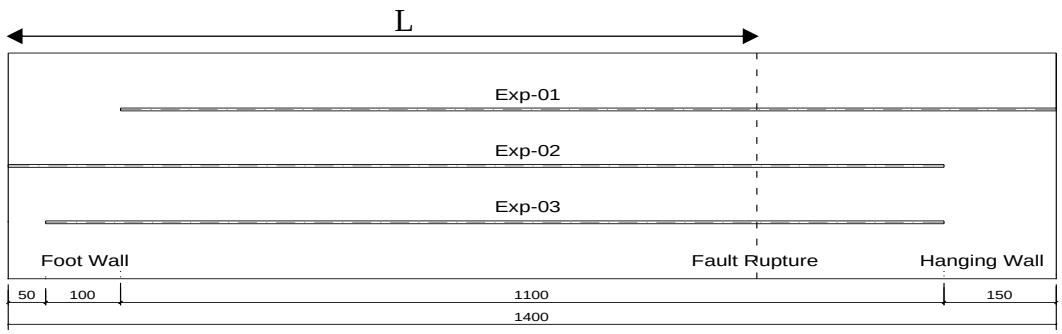

Figure 7. Illustration in plan showing boundary conditions for exploratory tests

Table 6. Summary of the exploratory tests (Fault displacement was continued up to 20-25D)

Test ID	Fixed Parameters	Variable Parameters	Remarks
Exp-01	Burial depth, H: 200mm (H/D = 40)	Material: Aluminium Alloy	Pipe at moving end wall fixity inclined upwards indicating buckling generated directly by movement of moving end wall. (Figure 8)
		Pipe length, L: 1250mm	
	Sand relative density: 77%	Boundary conditions: fixed to moving end wall – free at stationary end wall (Figure 7)	
Exp-02	Burial depth, H: 200mm (H/D = 40)	Material: Aluminium Alloy	Two regions of plasticity developed at intersection with fault rupture. Pipe either side of areas of plasticity observed as horizontal. (Figure 8)
		Pipe length, L: 1250mm	
	Sand relative density: 77%	Boundary conditions: free at moving end wall – fixed at stationary end wall (Figure 7)	
Exp-03	Burial depth, H: 200mm (H/D = 40)	Material: Brass Alloy	Final pipe location bearing on stationary end wall showing that the pipe moved. Analysis of results indicated the pipe was stationary initially.
		Pipe length, L: 1200mm	
	Sand relative density: 76%	Boundary conditions: free at moving end wall – free at stationary end wall (Figure 7)	

3.2. Large Displacement Tests

The test results show that bending strain is dominant close to the fault trace. However, it is expected that the axial strain would be greater than the bending strain far from the fault. According to test results, the bending strain is found to be critical in crossing the reverse fault and at large fault displacements, two different regions of plasticity and curvature develop in the pipeline similar to exploratory tests shown in Figure 8. The summary of large fault displacement tests is given in Table 7. The bending strain distribution of LD-01 and LD-02 are illustrated in Figure 9 and Figure 10. The pipeline end at the foot wall side is fixed in all three

directions (vertical, lateral and axial) while other pipe end is kept free at the hanging wall side as in Exp-02 (Figure 7).

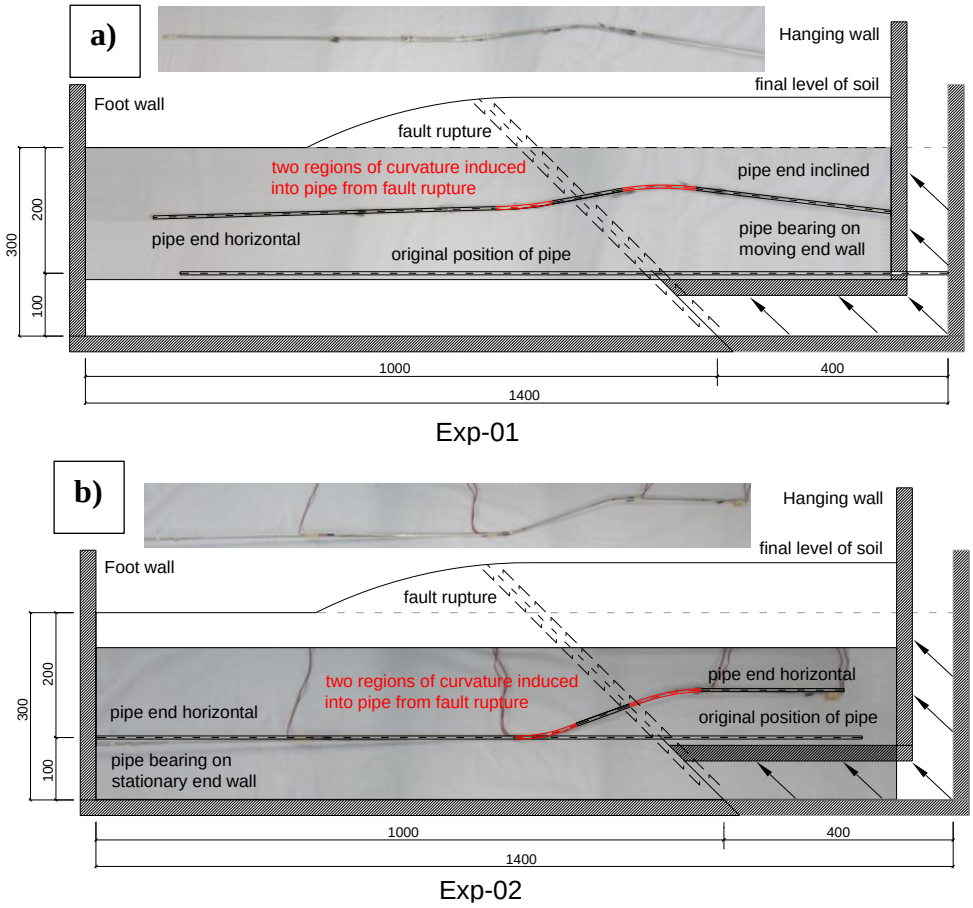

Figure 8. a) Photo and illustration showing that displaced shape for Exp-01 and b) Exp-02

3.3. Small Displacement Tests

Fifteen small displacement (SD) tests are performed in the scope of the experimental investigation. The parameters used in SD tests is summarised in Table 8. The strain gauge data is analysed by plotting the normalised bending strain individually (for every test) and jointly by comparison amongst the 15 tests (Figure 11-Figure 13). The boundary conditions of pipeline ends are the same as in Exp-02 (Figure 7). The pipeline end at the hanging wall side is kept free while other end is kept fixed in all three directions.

Table 7. Summary of relatively large fault displacement (LD) tests

Test ID	Fixed Parameters	Variable Parameters	Remarks
LD-01 (Repeat of Exp-02)	Burial depth: 200mm Sand relative density: 76% Pipe length: 1250mm	Material: Aluminium Alloy	Two locations of plasticity developed at intersection region with fault rupture. Lengths of pipe either side of plasticity observed as horizontal.
LD-02	Burial depth: 200mm Sand relative density: 75% Pipe length: 1250mm	Material: Brass Alloy	Two locations of plasticity developed at intersection region with fault rupture. Plasticity was not nearly as pronounced as LD-01. Pipe at moving end wall observed as inclined (5-10°).

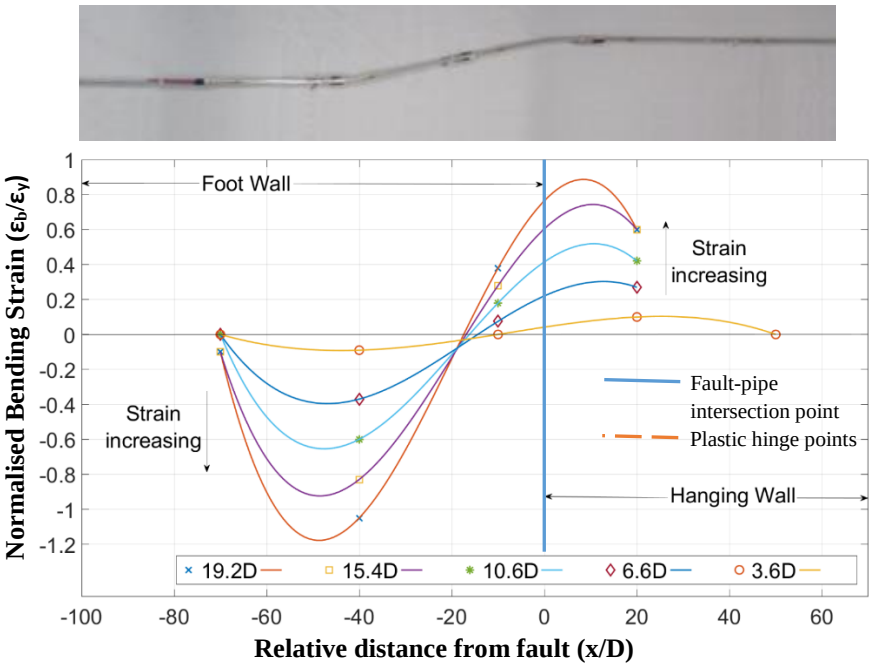

Figure 9. Plot of bending strain distribution of LD-01 shown against an image of the final displaced shape

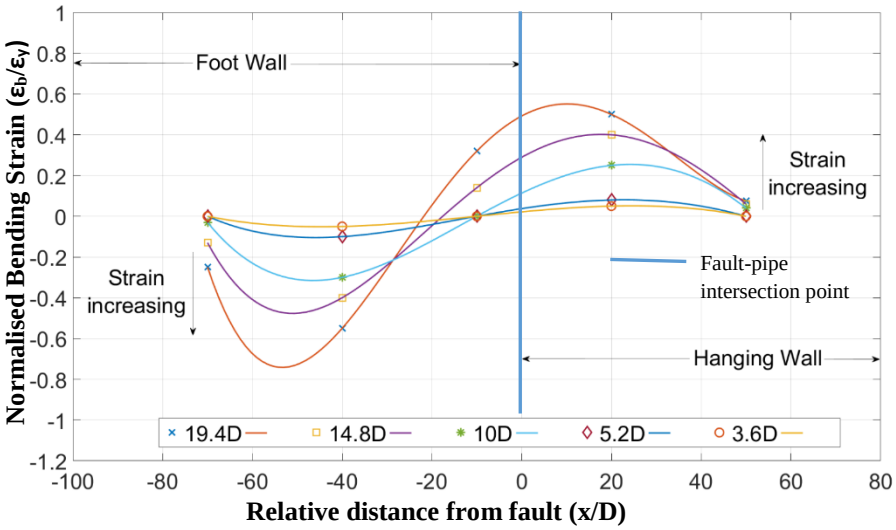

Figure 10. Plot of bending strain distribution of LD-02

Table 8. Summary of parameters used in small fault displacement tests

Test ID	Fixed Parameter	Variable Parameters	
	Relative Density (soil)	Material	Burial Depth, H
SD-01 SD-02	77% 76%	Brass Alloy	200mm (H/D = 40)
SD-03 SD-04	75% 76%	Brass Alloy	150mm (H/D = 30)
SD-05 SD-06	77% 75%	Brass Alloy	100mm (H/D = 20)
SD-07 SD-08	76% 77%	Brass Alloy	50mm (H/D = 10)
SD-09 SD-10	75% 75%	Brass Alloy	25mm (H/D = 5)
SD-11	77%	Aluminium Alloy	200mm (H/D = 40)
SD-12	77%	Aluminium Alloy	150mm (H/D = 30)
SD-13	76%	Aluminium Alloy	100mm (H/D = 20)
SD-14	76%	Aluminium Alloy	50mm (H/D = 10)
SD-15	77%	Aluminium Alloy	25mm

			(H/D = 5)

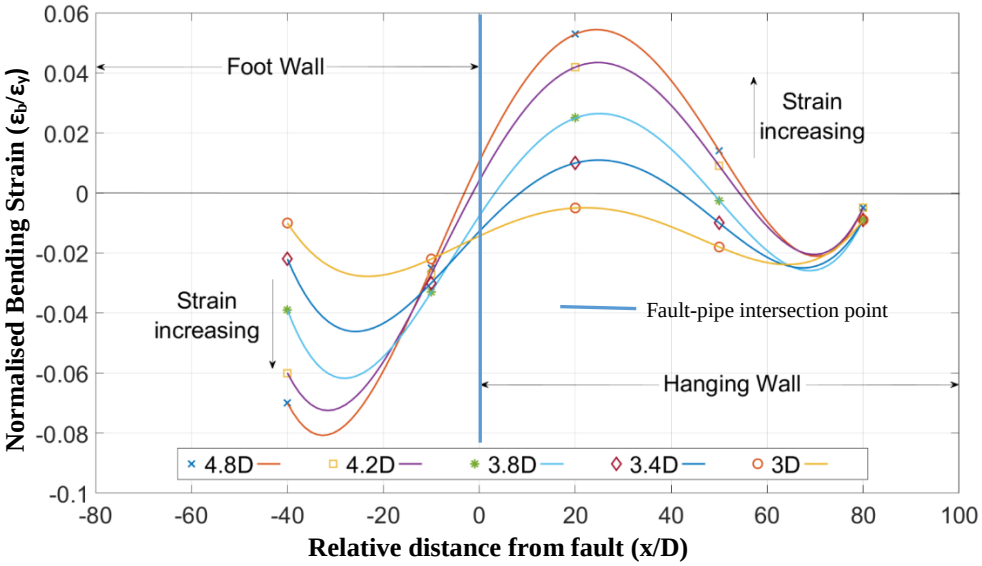

Figure 11. Plot of bending strain distribution of SD-10 (H/D=10)

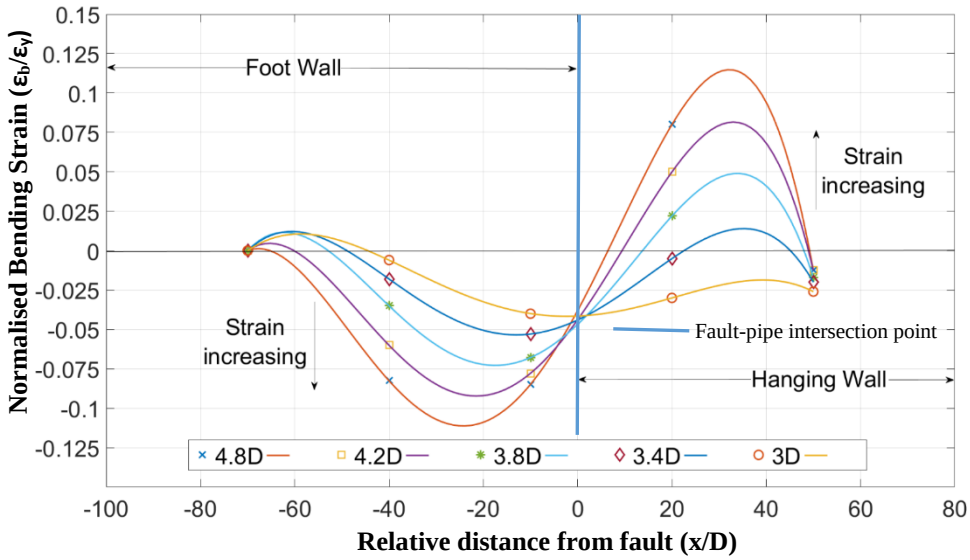

Figure 12. Plot of bending strain distribution of SD-01 (H/D=40)

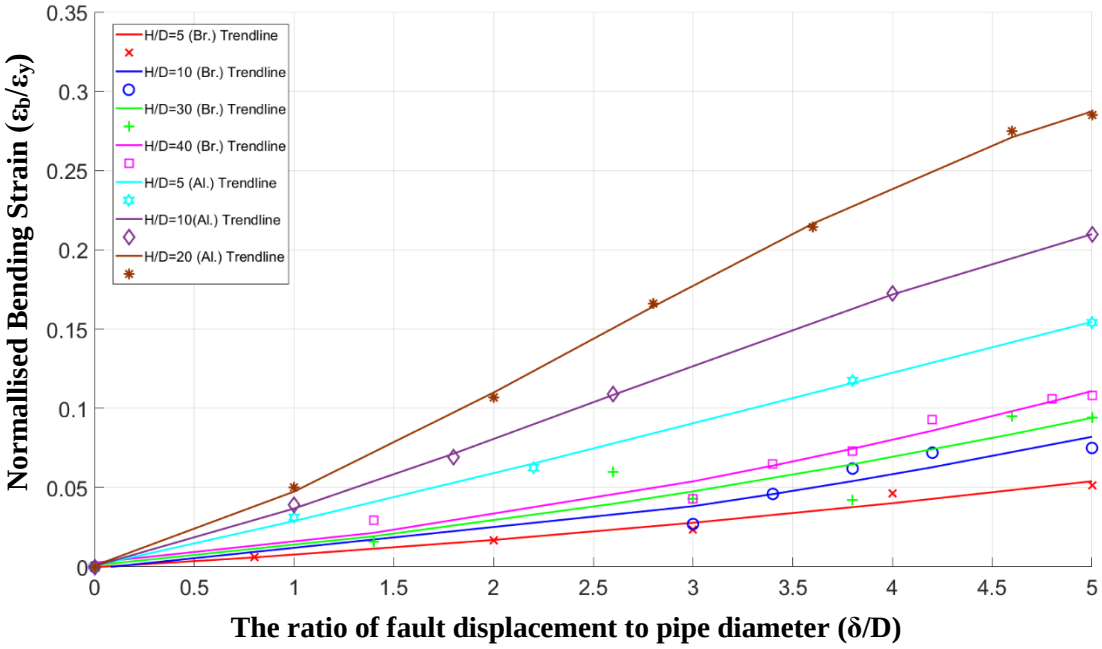

Figure 13. Plot of bending strain distribution of small displacement tests ($5 \leq H/D \leq 40$)

The test results demonstrate clearly that bending strains increase with depth. The results confirm trends predicted by theoretical and numerical analyses (Yun and Kyriakides, 1990; Joshi, 2009). The final deformed shapes of small displacement tests do not show obvious plasticity as per the large displacement tests. The normalised bending strains are dominant close to the fault as in the large displacement tests. Two curvatures develop in the pipeline similar to the exploratory tests. The plots of maximum normalized bending strains for different fault displacements are illustrated covering two materials and the burial depth range of $5 \leq H/D \leq 40$ (Figure 13). Points with different colours and shapes symbolize the normalized bending strains for different fault displacements while lines with various colours illustrate the trendlines for these points. An increase in H/D ratio results in an increase in soil stiffness surrounding the pipes. The increase in soil stiffness leads to an increase in relative soil-pipe stiffness (kD^4/EI). For the same H/D ratios, aluminium alloy pipe experience higher bending strain since relative soil-pipe stiffness for aluminium alloy pipe is higher than for brass alloy pipe. It is concluded that the bending strains in pipe increase with increasing relative soil-pipe stiffness (kD^4/EI).

4. Numerical Results

Soil-pipe interaction problems under faulting are generally considered as large deformation cases since excessive deformations occur in pipelines and soil surrounding pipelines during faulting. Due to large deformations in both soils and pipelines, this problem will exceed elastic limits of materials and consequently, nonlinear behaviours of materials need to be taken into account. Finite Element (FE) method is one of the best way to investigate these kinds of soil-structure interaction problems. In this study, ABAQUS v 6.14 software is used to model pipelines crossing reverse faults. This software is capable of simulating non-linear mechanical behaviour of soils and pipe materials, geometrical nonlinearity in the pipelines (distortions of the pipeline cross-section).

Numerical studies, which have been carried out in this study, can be grouped into two categories: 1) Three-dimensional (3D) Finite Element (FE) model of experimental setup, 2) 3D FE model of Case Study of the pipeline crossing reverse fault in San Fernando area (1971 San Fernando Earthquake).

The main purposes of numerical studies are as follows:

(1) To create a 3D FE model of experimental setup for pipelines crossing reverse faults and to validate the 3D FE analysis results with experimental results.
(2) To present a case study of the steel pipeline crossing reverse fault in San Fernando area during 1971 San Fernando Earthquake and to investigate the behaviour of field pipeline subjected to reverse fault.
(3) To introduce relative soil-pipe stiffness term (kD^4/EI) and to understand how it affects the behaviour of experimental and field pipelines.

4.1. Three-Dimensional (3D) Finite Element (FE) Model of Experimental Setup

A 3D FE simulation of the experimental setup of pipeline crossing reverse fault is created by using ABAQUS v 6.14. Two different stages are used to simulate the real field conditions: 1) Gravity loading and 2) Fault displacement. Gravity loading is applied to the whole model to simulate the stresses in the soil and on the pipe due to self-weight of the soil and pipe. In the second step, fault displacements with 45° fault dip angle (0.0148m in y direction and 0.0148m in –z direction) are applied incrementally to the right-hand side soil block (hanging wall) while left hand side soil block (foot wall) is kept fixed. Continuum elements (C3D8R) are used to model the soil and Mohr-Coulomb model, which is characterized by the friction angle (ϕ), the soil cohesion (c), the elastic modulus (E), Poisson's ratio (υ) and the dilatation angle (ψ), is chosen to represent the stress-strain relationship in soil. Shell elements (S4R) are used to model the pipeline and Isotropic Von Mises yield model is selected for the brass alloy pipe element. The interaction between the soil and pipe is modelled using both tangential and normal contacts. The tangential contact algorithm with a proper friction coefficient (μ) simulates the friction between the soil and pipe. The normal contact with selecting hard contact allows seperation of the pipe and soil surfaces. The soil-pipe interface friction parameter (μ) is considered equal to 0.3 as adopted in earlier studies (Vazouras et al., 2010; Vazouras et al., 2012). The parameters used in the FE model are given in Table 9.

The vertical boundary nodes (side walls) of the fixed parts are restricted in the horizontal direction and bottom wall of the fixed soil block are restricted as an encastre. The uniform fault displacement is applied in the external nodes of the moving part in vertical (y) and axial (z) directions as in the experimental model (Figure 8). The pipeline end at the foot wall side is fixed in all three directions (U1, U2, U3) and other pipe end is set free as in Figure 7 (Exp-02).

A fine mesh is used for the soil surrounding the pipeline, and the region close to the reverse fault trace, where the pipe and fault intersects (Figure 14a-b). Maximum stresses and strains in

the soil and pipeline are expected to develop in these parts. On the other hand, a coarser mesh is employed for the soil parts far from the fault trace (Figure 14b). The magnitude of the displacements in soil blocks are shown in Figure 14b. Figure 14c demonstrates the displacement profile of the pipeline. The longitudinal pipe strain distribution in the dashed red zone is shown in Figure 14d.

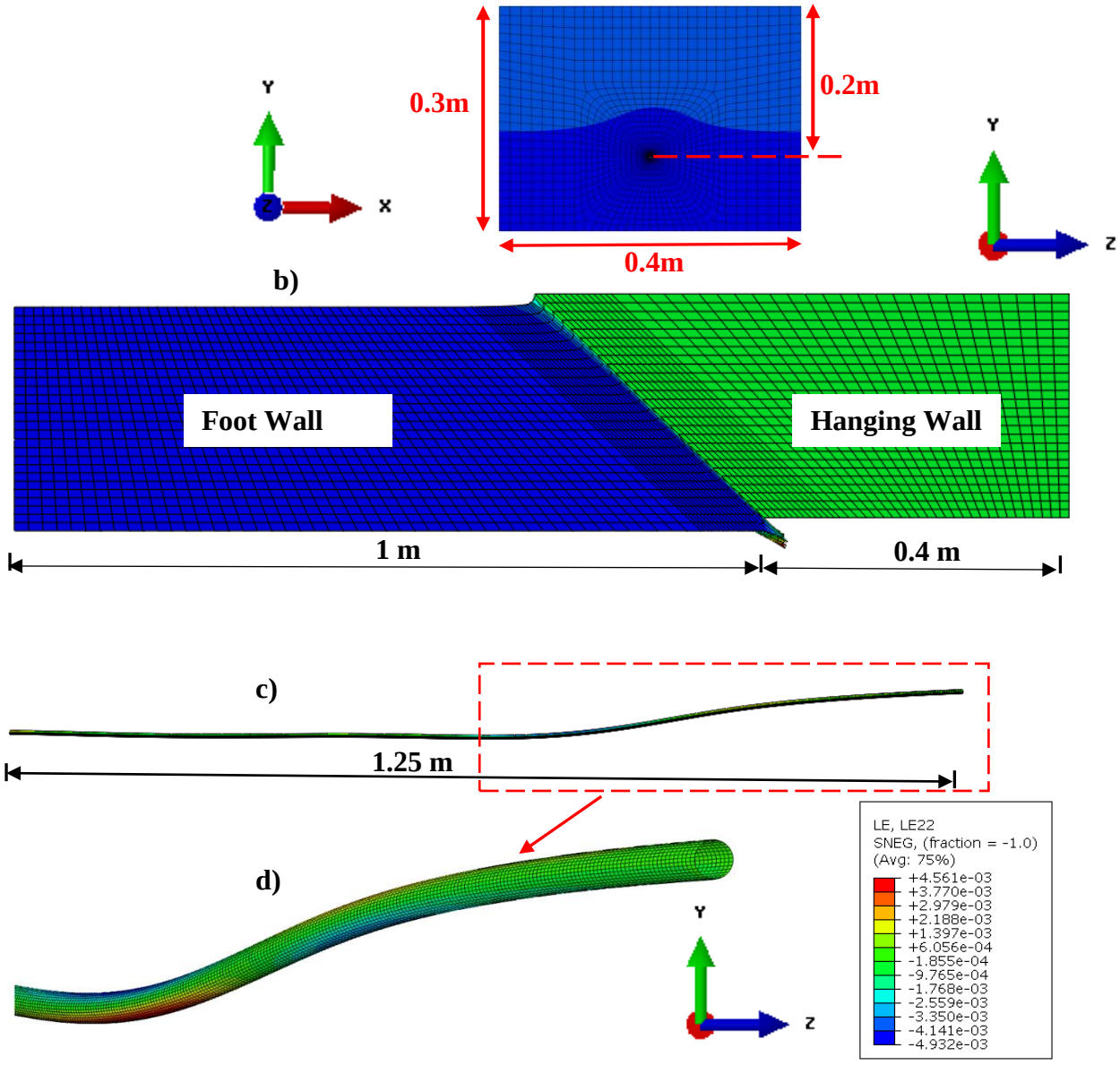

Figure 14. a) Cross-section of Three Dimensional (3D) Soil Continuum model, **b)** side view of the 3D FE model showing displacements of foot wall and hanging wall, **c)** displacement profile of the pipeline, **d)** longitudinal pipe strains in the dashed red zone

Table 9. Engineering properties of the soil and pipe and contact parameters used in the FE model

Soil: Red Hill Sand			
Elastic		***Plastic***	
E (Mpa)	0.25	**φ (°)**	34°
ϑ	0.4	**Ψ (°)**	1°
		c (kPa)	0
Pipe: Brass Alloy Pipe			
Elastic		***Plastic***	
E (Gpa)	84	**Yield Stress, MPa (σ_y)**	440
ϑ	0.3		
Contact			
Tangential		***Normal***	
μ	0.3	Hard Contact	

The pipe bending strains obtained from the FE model is presented by using non-dimensional parameters such as normalised pipe bending strain ($\varepsilon_b/\varepsilon_y$) and relative distance from the fault (x/D). Figure 15 demonstrates the graphs of $\varepsilon_b/\varepsilon_y$ versus x/D for 3D FE model and scale model test for that the pipeline is buried at 0.20m (H/D=40) and subjected to 6.6D (0.033m), 10.6D (0.053m) and 15.4D (0.077m) fault displacements. The magenta diamond, purple star and orange pentagon points represent the normalised bending strains obtained by strain gauges on the pipeline for 6.6D, 10.6D and 15.4D fault displacements, respectively. The black square, red circle and blue triangle points shows the distribution of normalised bending strains along the pipeline under 6.6D, 10.6D and 15.4D fault displacements, respectively and these data are obtained by 3D FE analysis.

The comparison of maximum and minimum normalised bending strain ($\varepsilon_b/\varepsilon_y$) obtained by LD-01 experiment and 3D FE analysis in Table 10. The maximal differences in experiment and 3D FE analysis results are included in the table. The maximal differences in $(\varepsilon_b/\varepsilon_y)_{max}$ range between 4% and 18.7% whereas the maximal differences in $(\varepsilon_b/\varepsilon_y)_{min}$ are between 0.13%-25.54%. The assumptions used in the 3D FE model are: 1) Soil medium is homogeneous and

2) Stress dependency behaviour of soil is not taken into account. These assumptions may be the reason behind these slight differences between experiment and 3D FE analysis results. However, the results show that the 3D FE model is fairly capable of simulating the experimental model.

Table 10. Comparisons of maximum and minimum normalised bending strains (εb/εy) obtained by LD-01 experiment and 3D FE analysis

	Experiment		**3D FE**		**Maximal Differences**	
δ/D	$(\varepsilon_b/\varepsilon_y)_{max}$	$(\varepsilon_b/\varepsilon_y)_{min}$	$(\varepsilon_b/\varepsilon_y)_{max}$	$(\varepsilon_b/\varepsilon_y)_{min}$	$(\varepsilon_b/\varepsilon_y)_{max}$ (%)	$(\varepsilon_b/\varepsilon_y)_{min}$ (%)
6.6	0.3028	-0.3955	0.336	-0.396	10.96	0.13
10.6	0.5187	-0.654	0.498	-0.614	3.99	6.12
15.4	0.7432	-0.924	0.882	-1.16	18.68	25.54

4.2. Case Study of the Pipeline Crossing Reverse Fault (1971 San Fernando Earthquake)

Large deformations were imposed to gas and water transmission pipelines crossing reverse fault during 1971 San Fernando earthquake. Severe damages including shell (local) buckling and tensile failure were observed along the steel transmission line. Steel pipelines with 0.40m diameter experienced shell buckling due to compressive forces imposed on due to fault movement. Most of the pipelines in the San Fernando area were located in alluvial sand and gravel at depths between 0.75 and 1.5m (SCGC, 1973). The operating pressure for gas pipelines was 0.414 MPa.

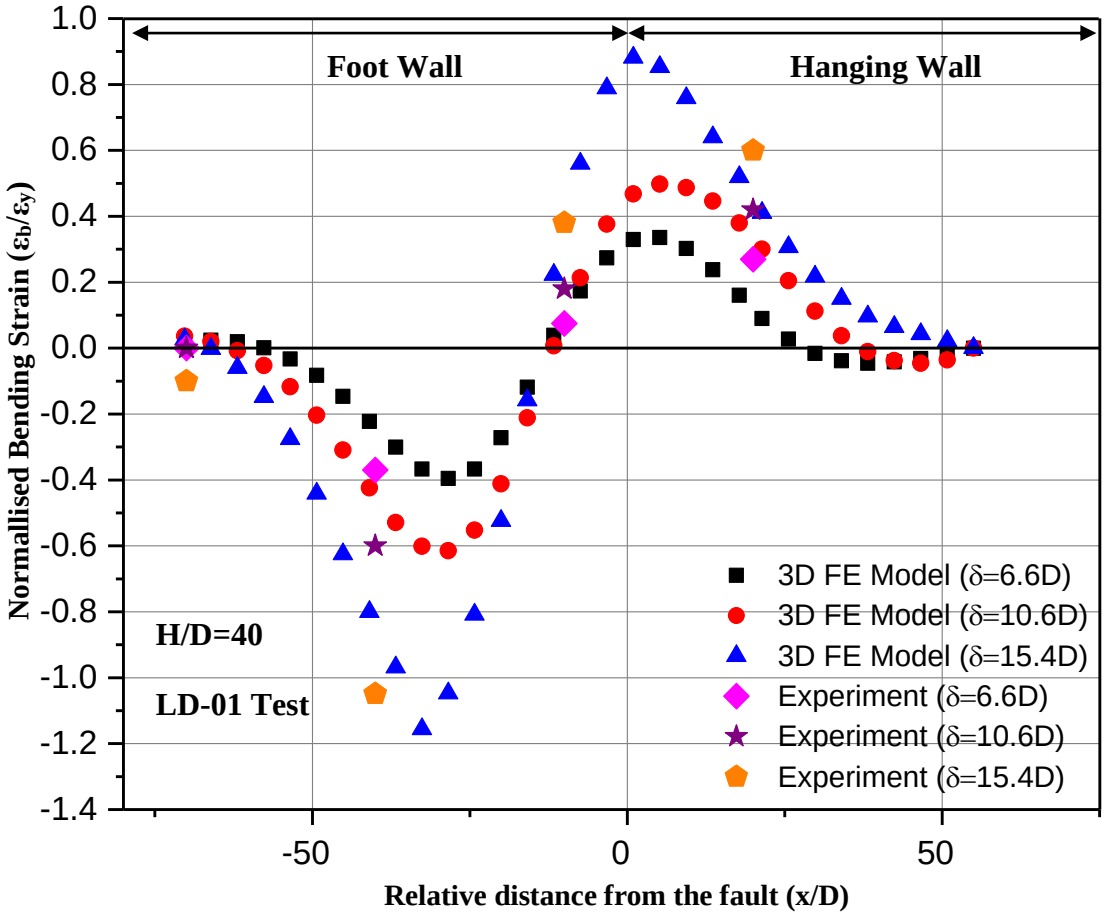

Figure 15. Plots of normalised pipe bending strains ($\varepsilon_b/\varepsilon_y$) versus relative distance from fault (x/D)

A 3D quasi-static nonlinear analysis of the 0.4m diameter pipeline crossing the reverse fault in the San Fernando area is performed by applying fault displacements incrementally. Three different loading steps are used to simulate the real field conditions: 1) gravity loading, 2) internal pressure of the pipe, and 3) fault displacement. Firstly, gravity loading step is used to calculate stresses in the soil and on the pipeline due to their self-weight. In the second step, an internal pressure of 0.414 MPa is applied to inner wall surface of the pipe. These first two stages are used to simulate operational stresses in the pipe. Finally, fault displacements (1.90m in –z direction and 1.40m in y direction) are applied to right hand side soil part and other soil part is restrained in every directions. In order to take into account boundary conditions in the field, equivalent soil springs are used at the both end sides of the pipe (Figure 17b). The equivalent boundary springs are capable of taking into account soil-pipe axial interaction forces

along the unanchored length. The force-elongation relationship for the equivalent boundary spring is calculated by using equations developed by Liu et al. (2004) and given in Figure 16. The initial imperfection of the pipeline was not taken into account in the analysis. Such imperfections may significantly influence the occurrence of local buckling. This can be considered as a limitation of FE model.

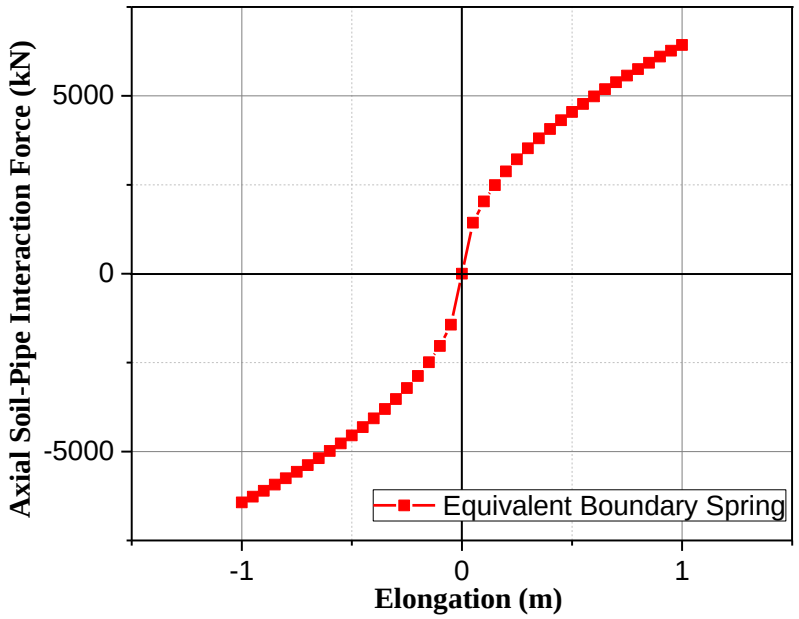

Figure 16. Force-elongation (F-δ) relationship for equivalent boundary spring

In the 3D FE model, pipeline is assumed to be buried in medium dense sand with 38° internal friction angle at 1.0m depth. A steel pipeline with 0.40m diameter and 0.008m wall thickness is used to simulate the pipeline crossing faults in San Fernando area. Engineering properties of the soil and pipeline, characteristics of the fault and the parameters used in the 3D FE model are given in Table 11.

The cross-section of 3D soil continuum model is shown in Figure 17a. The side view of the soil continuum and pipe showing magnitudes of the displacements are demonstrated in Figure 17b-c. The longitudinal pipe strain distribution in the dashed red zone is shown in Figure 17d. A fine mesh was utilized for the central part of the pipeline and soil blocks (regions close to the fault trace), where maximum stresses and strains are expected. A total of 50 shell elements

around the cylinder circumference are used whereas in longitudinal direction, the size of shell elements is selected equal to 1/26 pipeline outer diameter (D). The more refined finite element mesh is used for the soil region near the fault and coarser mesh for the region far from the fault.

Table 11. Engineering properties of the soil and pipe and contact parameters used in the FE model

Soil: Alluvial Sand and Gravel			
Elastic		***Plastic***	
E (Mpa)	20	**φ (°)**	38°
ϑ	0.4	**Ψ (°)**	1°
		c (kPa)	1
Pipe: Steel Pipe			
Elastic		***Plastic***	
E (GPa)	210	**Yield Stress, MPa (σ_y)**	250
ϑ	0.3		
Contact			
Tangential		***Normal***	
μ	0.3	Hard Contact	

As seen in the Figures 16a-b, a fine mesh is employed for the soil surrounding pipe and the regions close to the reverse fault trace. On the other hand, a coarser mesh is used for the soil parts far from the fault trace (Figure 17b). The length of model is selected as 50 m (125D) and it is greater than the proposed length (60D) in Vazouras et al. (2010).

Figure 18 shows the variation of longitudinal pipe strain at the compression side of the buckled area (point A) for different values of normalised fault displacements (δ/D) ranging from 0.34 to 5.9D. Strain localization occurs at a certain point due to shell (local) buckling as δ/D increases. The results indicate that significant pipe deformations occurs due to the development of local buckling on the pipe wall at the compression side of the buckled area.

It is of interest to compare our approach with that of Liu et al. (2016). In both cases equivalent boundary approach and similar pipe models are used. However, in our approach soil medium is modelled as continuum elements whereas of Liu et al. (2016) modelled the pipe-soil interaction as a non-linear soil spring.

Liu et al. (2016) carried out a parametric study using 3D FE model in order to understand effects of steel properties on the local buckling response of high strength pipelines crossing reverse faults. In their study, local buckling (wrinkling) occurs in the pipe at even small fault displacements. For fault displacements larger than 4.03D, wavy distribution of longitudinal strain becomes more severe and it peaks abruptly at about δ/D of 5.55D, see Figure 18.

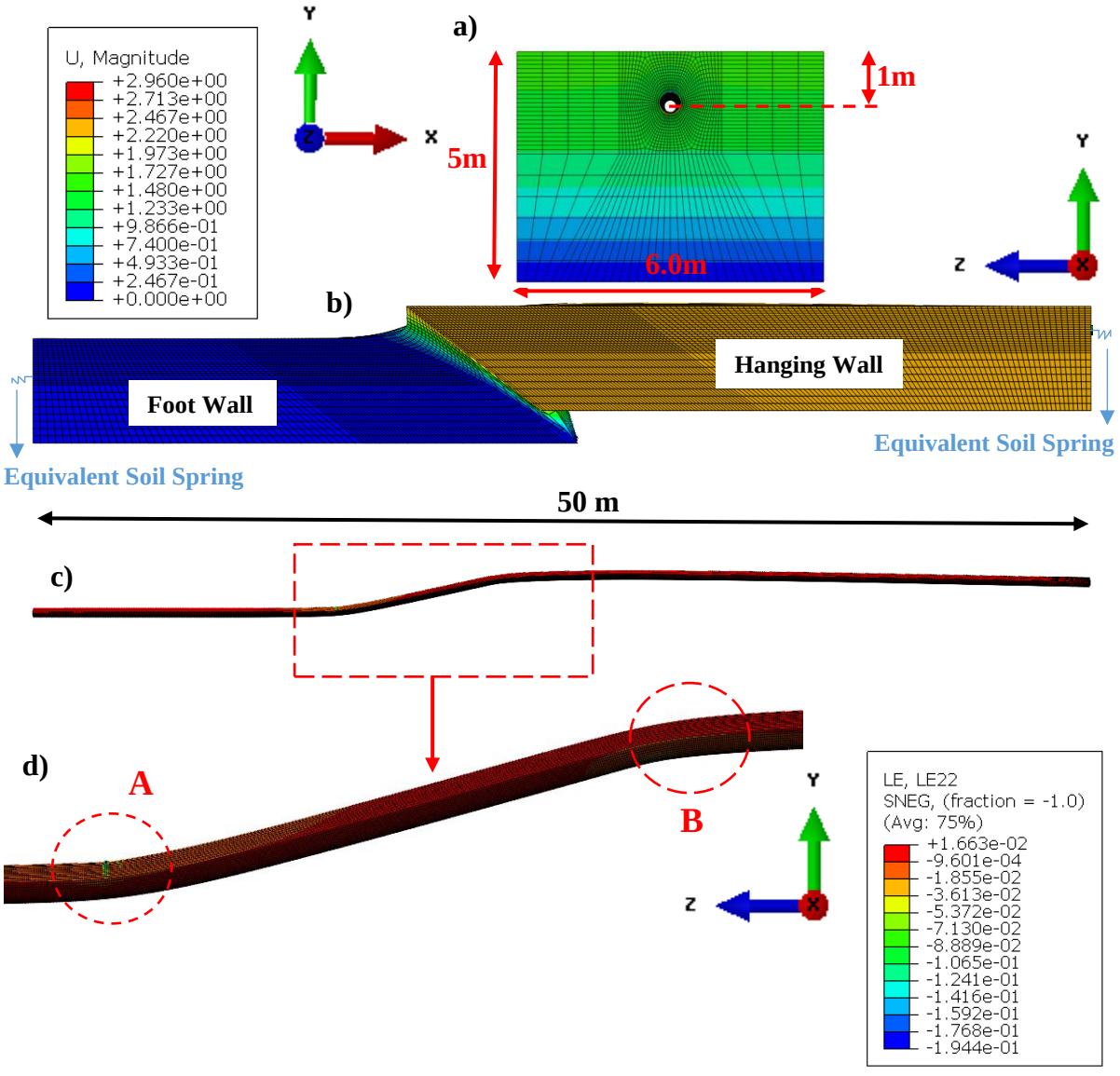

Figure 17. a) Cross-section of Three-Dimensional (3D) Soil Continuum model, **b)** side view of the 3D FE model showing displacements of foot wall and hanging wall, **c)** displacement profile of the pipeline, **d)** longitudinal pipe strains in the dashed red zone, **e)** compression side of Point A, **f)** compression side of Point B

The variation of longitudinal pipe strains at the tension side of the buckled area (point A) for different values of δ/D is demonstrated in Figure 19. Due to the occurrence of local buckling, pipe deformation concentrates around the buckled area resulting in the development of localized wrinkling pattern. As the imposed fault displacement is increased, significant local strains including compressive and tensile strains develop at buckled area due to pipe wall folding. Consequently, the local tensile strains at the buckled area are significantly increased.

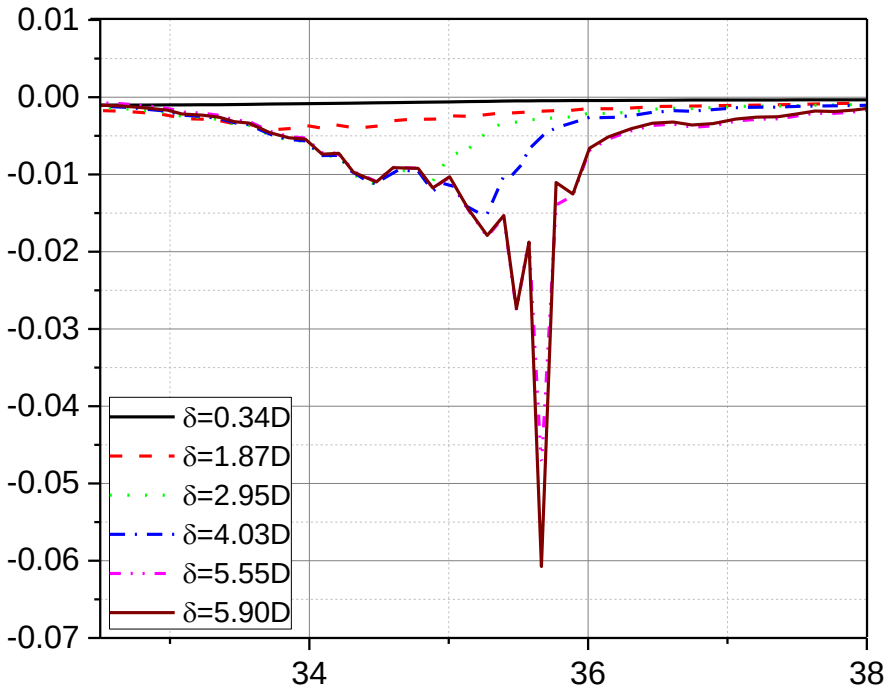

Figure 18. Variation of longitudinal strain at the compression side of the buckled area (Point A) for values of normalised fault displacement (δ/D) from 0.34D to 5.90D

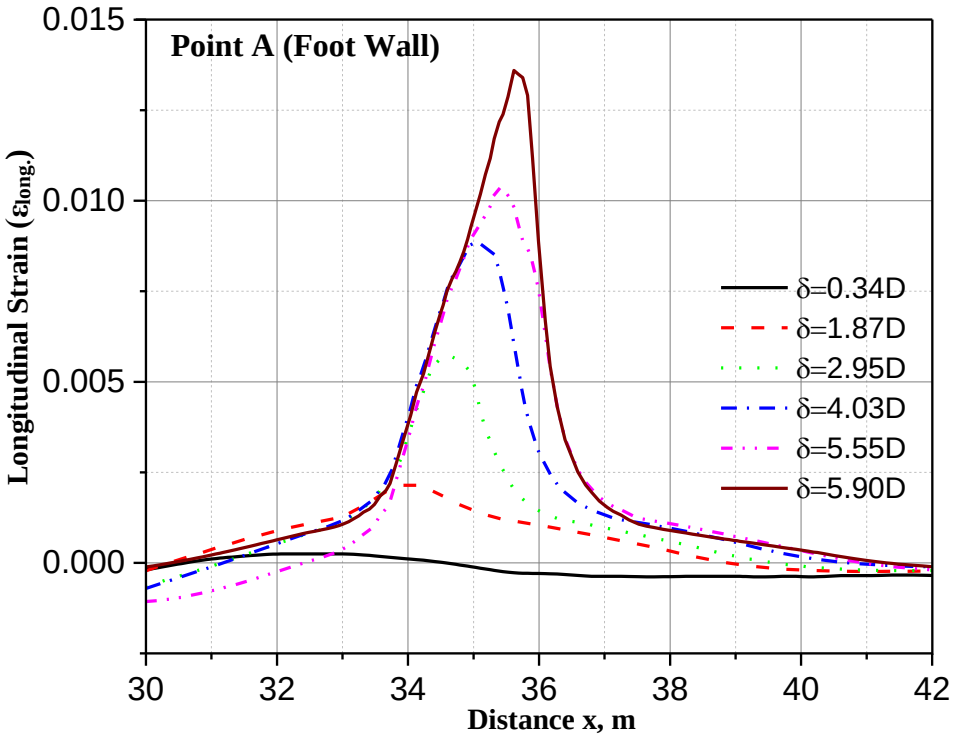

Figure 19. Variation of longitudinal strain at the tension side of the buckled area (Point A) for values of normalised fault displacements (δ/D) from 0.34D to 5.90D

Figure 20 shows the variation of maximum normalised longitudinal (tensile, compressive) strains ($\varepsilon_{long.}/\varepsilon_y$) for different values of normalised fault displacements (δ/D). Experimental pipelines do not experience local buckling or tensile failure whereas the field pipeline experiences significant damages due to local buckling and tensile failure. This different behaviour of field and experimental pipelines is due to that they have different values of relative soil-pipe stiffness (kD^4/EI). In order to obtain similar pipe behaviour, kD^4/EI ratio of experimental should be kept close to the values of field pipelines. Table 12 shows kD^4/EI values for the experimental pipelines (brass and aluminium alloy) and the field pipeline (steel pipeline in San Fernando area). Soil stiffness values (k) for each tests were calculated based on ultimate bearing soil force formulae and yield displacement values proposed by ASCE 1984 Guidelines. The critical strain equation for local buckling is given on the graph in Figure 20. The design equation was initially proposed by Gresnigt (1986) and is later adopted by CSA Z662 specification.

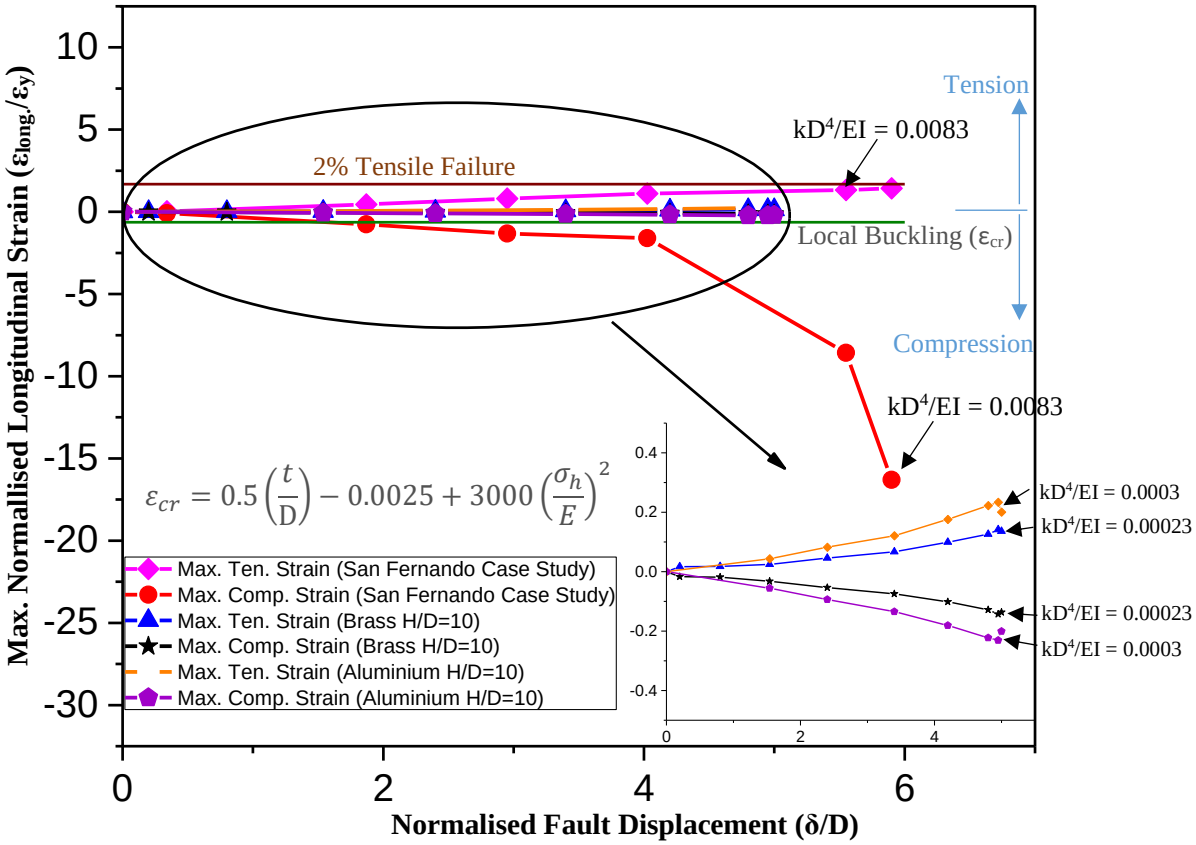

Figure 20. Maximum normalised longitudinal strain ($\varepsilon_{long.}/\varepsilon_y$) versus normalised fault displacement (δ/D) for the small-scale experiments and the 1971 San Fernando case study

Table 12. Relative soil-pipe stiffness values for the experimental pipelines and the field pipeline in San Fernando area

Pipelines	Material	D (m)	t (m)	H (m)	H/D	EI (kNm^2)	kD^4/EI
Experimental	Aluminium Alloy	0.005	0.00045	0.025	5	0.00111	0.0002
	Brass Alloy	0.005	0.00045	0.025	5	0.00141	0.0001
	Aluminium Alloy	0.005	0.00045	0.05	10	0.00111	0.0003
	Brass Alloy	0.005	0.00045	0.05	10	0.00141	0.00023
	Aluminium Alloy	0.005	0.00045	0.1	20	0.00111	0.0006
	Brass Alloy	0.005	0.00045	0.1	20	0.00141	0.0005
Field	Steel	0.4	0.008	1	2.5	39756.51	0.0083

5. Discussions and Conclusions

A new 1-g scale testing apparatus for physical modelling of pipelines crossing reverse faults is developed and described in detail. Scaling laws and similitude relations are derived for the small-scale model of pipelines crossing strike-slip faults. The most important parameter governing the behaviour of pipelines is relative soil-pipe stiffness. Experimental data obtained from the tests are consistent with the field observation and numerical studies.

Three-dimensional Finite Element (3D FE) analysis of the experiments set-up were carried out and compared with the test results. Furthermore, the case study of the 0.4m diameter steel gas pipeline crossing reverse fault in San Fernando area (during 1971 San Fernando earthquake) is performed. 3D FE model of this pipeline is created and FE analysis is carried out to have a deeper understanding about the behaviour of field pipelines crossing reverse faults.

The main conclusions that are derived from the study are as follows:

1) For a constant pipe diameter, bending strain increases with increasing H/D ratios. It is therefore suggested that the pipes should be buried at a shallow depth in the vicinity of the fault zone in order to minimize compressive and bending strains.
2) The test setup used in the study represents fault crossing angle of 90^0 and fault dip angle of 45^0. For this case, bending strain is dominant in the vicinity of the fault where the pipe is subjected to reverse fault rupture. As expected and observed in the experiments, the critical zone for bending strain is the fault crossing zone where double curvature develops leading to plastic deformation and yielding.
3) In reverse fault cases, two different curvature region ($R_2>R_1$) occurs due to asymmetric soil loading. This loading condition develops due to difference between ultimate uplift and bearing soil resistance. In most cases, larger bending strains develop within pipeline at foot wall side of the reverse fault.
4) The case study of the pipeline crossing reverse fault in San Fernando area shows that pipelines are vulnerable to compressive forces arising due to reverse fault movements. The initiation of local buckling in the pipe wall develops at smaller δ/D ratios. Significant tensile strain develops at the buckled area due to folding of the pipe wall.
5) It is concluded that pipes experience larger longitudinal strains with increasing relative soil-pipe stiffness ratio which can be represented by a non-dimensional group kD^4/EI. 3D FE analysis results also confirm the relevance of this group. In order to replicate reverse fault induced collapse or failure mechanisms, kD^4/EI ratio in scale-model tests should be kept consistent with those values for field pipelines.

Acknowledgments
The authors wish to thank the former UG project students Francesca Draper and William Mahoney, for their assistance in designing the test apparatus and conducting tests. The authors would also like to acknowledge the contribution of Dr Suresh R Dash (Assistant Professor, Indian Institute of Technology, Bhubaneswar) for support in carrying out some analysis.

References:

Abdoun T. H., Ha, D., O'Rourke, M. J., Symans, M. D., O'Rourke, T. D., Palmer, M. C., and Stewart, H. E. (2009). Factors influencing the 41odelling of buried pipelines subjected to earthquake faulting. Soil Dynamics and Earthquake Engineering, 29, 415– 427

ASCE (1984). Guidelines for the Seismic Design of Oil and Gas Pipeline Systems, Committee on Gas and Liquid Fuel Lifelines, American Society of Civil Engineers (ASCE), US, Nyman, D. J.

Bhattacharya S., Lombardi D., Dihoru L., Dietz M.S., Crewe J.C., and Taylor C.A. (2012). Model Container Design for Soil-Structure Interaction Studies. Role of seismic testing facilities in performance-based earthquake engineering. The Netherlands:Springer; 2012; 135-58

Bolton M.D. (1986). The strength and dilatancy of sands, Geotechnique 36(1):65-78

Bolton, M. D., Gui, M. W., & Phillips, R. (1993). Review of miniature soil probes for model tests. Proceedings of 11th South East Asia Geotechnical Conference, (pp. 85-91). Singapore.

Bouzid D.A., Bhattacharya S., Dash S.R. (2013). Winkler springs (p-y curves) for pile design from stress-strain of soils: FE assessment of scaling coefficients using the Mobilized Strength Design concept, Geomechanics and Engineering, Vol. 5, No.5, 379-399

Canadian Standard Association. Oil and gas pipeline systems, CSA-Z662. Mississauga, Ontario, Canada; 2007.

Denys, R. (2000). Pipeline Technology Volume 2. Brugge: Elsevier Science BV.

Dickin E.A. and Leuoy C.F. (1983). Centrifuge Model Tests on Vertical Anchor Plates, ASCE J Geotechnical Engineering, 109(12): 1503–1525

Earthquake Spectra (2000). Kocaeli, Turkey, Earthquake of August 17, 1999. Reconnaissance Report, Earthquake Spectra, Vol. 16, no. S1, December 2000, pp. 1-461

EERI (1999). The Izmit (Kocaeli), Turkey Earthquake of August 17 1999. EERI Special Earthquake Report, October 1999

EERI (1999). The Chi-Chi, Taiwan Earthquake of September 21, 1999. EERI Special Earthquake Report, December 1999

EERI (2008). The Wenchuan, Sichuan Province, China, Earthquake of May 12, 2008. EERI Special Earthquake Report, October 2008

EEFIT (2009). The L'aquila, Italy Earthquake of 6 April 2009. A Preliminary Field Report by EEFIT

EERI (2010). The Mw 8.8 Chile Earthquake of February 27, 2010. EERI Special Earthquake Report, June 2010

Gordon, F. P., & Lewis, J. D. (1980). The Meckering Earthquake and Caligri Earthquake of October 1968 and March 1970. Geological Suvey of Western Autraliam, Bulletin 126.

Gresnigt AM. Plastic design of buried steel pipes in settlement areas. HERON 1986; 31(4):1–113.

Guo E., Shao G. & Liu H. (2004). Numerical Study on damage to buried oil pipeline under large fault displacement. Proceedings of 13th World Conference Earthquake Engineering.

Ha, D., Abdoun, T. & O'Rourke, M. J. (2008). Soil-Pipeline Interaction Behaviour under Strike-Slip Faulting. Geot. Earthq. Eng. & Soil Dynamics IV GSP 181 © 08 ASCE

Ha, D., Abdoun T. H., O'Rourke, M. J., Symans, M. D., O'Rourke, T. D., Palmer, M. C., and Stewart, H. E. (2008). Buried high-density polyethylene pipelines subjected to normal and strike-slip faulting – a centrifuge investigation. Canadian Geotechnical Journal, 45, 1733-1742

Ha, D., Abdoun, T.H., O'Rourke, M.J., Symans, M.D., O'Rourke, T.D., Palmer, M.C., Stewart, H.E. (2010). Earthquake Faulting Effects on Buried Pipelines-Case History and Centrifuge Study. Journal of Earthquake Engineering. 14:5, 646-669

International Technical Committee TC2 (2005). Catalogue of scaling laws and similitude questions in centrifuge 43odelling.

Johansson J., Konagai K. (2005). Shear band development length and implications for rupture propagation through soil. Proceedings of the JSCE Earthquake Engineering Symposium, Volume 28, pp. 82.

Joshi, S. S. (2009). Analysis of buried pipelines subjected to reverse fault motion. M. Tech thesis. Indian Institute of Technology Kanpur, India

Karamitros D.K., Bouckovalas G.D. & Kouretzis G.P. (2007). Stress Analysis of Buried Steel Pipelines at Strike-slip Fault Crossings. Soil Dynamics and Earthquake Engineering, Vol. 27, pp. 200–211.

Karamitros D.K., Bouckovalas G.D., Kouretzis G.P., and Gkesouli V. (2011). An Analytical Method for Strength Verification of Buried Steel Pipelines at Normal Fault Crossings. Soil Dynamics and Earthquake Engineering, Vol. 31(11), pp. 1452-1464.

Kelly, R. B., Houlsby, G. T. & Byrne, B. W. (2006). A comparison of field and lab tests of caisson foundation in sand and clay. Geotechnique 56, No. 9, 617–626

Kennedy, R. P., Chow, A. W. and Williamson, R. A. (1977). Fault movement effects on buried oil pipeline. Transportation Engineering Journal, ASCE 103:5, 617-633.

Leblanc C., Byrne B.W., Houlsby G.T. (2010). Response of stiff piles random two-way lateral loading. Geotechnique 60(9):715-721

Lim M. L., Kim M. K., Kim T. W., and Jang J. W. (2001). The 44odelling analysis of buried pipeline considering longitudinal permanent ground deformation. In Pipeline 2001: Advances in Pipelines Engineering & Construction (San Diego, California), vol. 3, edited by J. P. Castronovo, 107, ASCE.

Lee J. W., Hamada M., Tabuchi G., Suzuki K. (2004). Prediction of fault rupture propagation based on physical model tests in sandy soil deposit. 13th World Conference on Earthquake Engineering, Paper No: 119, August 1-6, Vancouver, Canada

Lin T.J., Liu G.Y., Chung L.L., Chou C.H., Huang C.W. (2012). Verification of Numerical Modeling in Buried Pipelines under Large Fault Movements by Small-Scale Experiments. In Proc. 15WCEE, 2012, 9, 6685 – 6693.

Liu, A. W., Hu, Y. X., Zhao, F. X., Li, X. J., Takada, S., Zhao, L. (2004). An equivalent boundary method for the shell analysis of buried pipelines under fault movement. ACTA Seismologica Sinica. 17 (Suppl. 1), pp. 150-156. 2004. DOI: 10.1007/s11589-004-0078-1

Liu, X., Zhang, H., Li, M., Xia, M., Zheng, W., Wu, K., Han, Y., Effects of steel properties on the local buckling response of high strength pipelines subjected to reverse faulting, Journal of Natural Gas Science & Engineering (2016), Vol 33, P. 378-387.

Meyersohn, W. D. (1991). Analytical and Design Considerations for the Seismic Response of Buried Pipelines. M.S. thesis, Cornell University, USA.

National Research Council (1991). The March 5, 1987, Ecuador Earthquakes: Mass Wasting and Socioeconomic Effects. Washington, DC: The National Academies Press. Doi:https://doi.org/10.17226/1857.

Newmark, N. M., and Hall W. J. (1975). Pipeline design to resist large fault displacements, Proceedings of the U.S. National.

O'Rourke, M., Vikram, G. and Abdoun, T. (2003). Centrifuge modeling of buried pipelines. Proceedings of the Sixth U.S. Conference and Workshop on Lifeline Earthquake Engineering, August 10-13, 2003, Long Beach, CA. 757-768.

O'Rourke, M. , Gadicherla, V. , and Abdoun, T. (2005). Centrifuge 45odelling of PGD response of buried pipe. Earthquake Eng. Eng. Vib. 4 (1), 69–73

O'Rourke, T.D. and A. Bonneau (2007). Lifeline Performance Under Extreme Loading During Earthquakes",Earthquake Geotechnical Engineering ,K.D. Pitilakis, Ed., Springer, Dordrecht, Netherlands, 407-432

O'Rourke, T.D. (2010). Geohazards and Large Geographically Distributed Systems, 2009 Rankine Lecture, Geotechnique, Vol. LX, No. 7, July, 2010, pp. 503-543.

Ovesen, N.K. (1981). Centrifuge Tests of the Uplift Capacity of Anchor', Proc. Of the Tenth International Conference on Soil Mechanics and Foundation Engineering, Stockholm, pp.712-722

Palmer, M.C., O'Rourke, T.D., Stewart, H.E., O'Rourke, M.J., and Symans, M. (2006). Large displacement soil-structure interaction test facility for lifelines. Proc, 8th US National Conf. Commemorating the 1906 San Fransisco Earthquake, EERI, San Fransisco

Sakanoue T., and Yoshizaki K. (2004). A Study on Eartquake-Resistant Design for Buried Pipeline Using Lightweight Backfill. 13th World Conference on Earthquake Engineering, Vancouver, B.C., Canada, August 1-6, 2004, Paper No.2389

SCGC (1973). Earthquake Effects on Southern California Gas Company Facilities. San Fernando, California Earthquake February 9, 1971, Vol 2, Southern California Gas Company, US Dept. of Commerce, Washington. D.C., 59-66

Stone, K. J. L. and Wood, D.M. (1992). Effects of dilatancy and particle size observed in model tests on sand, Soils and Foundations, JSSMFE, Vol. 32, No 4., pp. 43-57

Schiff, A.J. & Holzer, T.L. (1998). The Lorna Prieta, California, Earthquake of October 17, 1989-Lifelines. Performance of the Built Env. U.S. Geological Survey Prof Paper 1552-A.

Takada, S., Hassani, N. and Fukuda, K. (2001). A new proposal for simplified design of buried steel pipes crossing active faults. Earthquake Engineering and Structural Dynamics 30, 1243-1257

Trifonov O.V. and Cherniy V.P. (2010). A semi-analytical approach to a nonlinear stress-strain analysis of buried steel pipelines crossing active faults. Soil Dynamics and Earthquake Engineering, 30(10), 1298-1308.

Trifonov O.V., Cherniy V.P. (2012). Elastoplastic stress-strain analysis of buried steel pipelines subjected to fault displacements with account for service loads. Soil Dynamics and Earthquake Eng. 2012, 33(1), 54-62.

Trifonov O.V. (2015). Numerical Stress-Strain Analysis of Buried Steel Pipelines Crossing Active Strike-Slip Faults with an Emphasis on Fault Modeling Aspects. J. Pipeline Syst. Eng. Pract. 2015, 6(1), 04014008.

Vazouras, P., Karamanos, S. A., and Dakoulas, P. (2010). Finite element analysis of buried steel pipelines under strike-slip fault displacement, Soil Dyn. Earthq. Eng., 30 (11), 1361–1376

Vazouras, P., Karamanos, S. A., and Dakoulas, P. (2012). Mechanical 46odelling of buried steel pipes crossing active strike-slip faults, Soil Dyn. Earthq. Eng., 41, 164–180

Vazouras, P., Dakoulas, P., Karamanos, S. A. (2015). Pipe–soil interaction and pipeline performance under strike–slip fault movements, Soil Dyn. Earthq. Eng., 72, 48–65

Wang L., R., L., and Yeh Y. (1985). A refined seismic analysis and design of buried pipeline for fault movement. Earthquake Engineering and Structural Dynamics 13(1), 75-96.

Wroth, C. P., Randolph, M. F., Houlsby, G. T. & Fahey, M. (1979). A review of the engineering properties of soils with particular reference to the shear modulus, Report CUED/D-SOILS TR75, Cambridge: University of Cambridge

Xie, X., Symans, M.D., O'Rourke, M.J., Abdoun, T.H., O'Rourke, T.D., Palmer, M.C., and Stewart, H.E. (2011). Numerical 47odelling of buried HDPE pipelines subjected to strike-slip faulting. Journal of Earthquake Engineering, 15(8): 1273– 1296.

Yun, H., & Kyriakides, S. (1990). On the beam and shell modes of buckling of buried pipelines. Soil Dynamics and Earthquake Engineering 9*:* 179-193.

Zhang L., Zhao X., Yan X., Yang X. (2016). A new finite element model of buried steel pipelines crossing strike-slip faults considering equivalent boundary springs. Engng Struct., 123, 30 – 44.

APPENDIX A

Table A-1. Pipeline Failure Case Studies relevant to Fault crossing

Earthqu.		Fault Characteristics					Geology of Area	Pipe Characteristics											Reference
1)Year	2) Location	3) Type	4) Name	5) Maximum Displacement H-V (mm)	6) Length (km)	7) Magnitude of Accompanying Earthquake	8) Geology Description	9) Name	10) Nature of Content	11) Diameter (mm)	12) Material & Condition	13) Yield Stress (Mpa)	14) Ultimate Tensile Stress (Mpa)	15) Fault Offset (δ) m	16) D/t	17) H/D	18) δ/D	19) Type of Failure	
1954	Kern County	Left-Lateral Reverse	*White Wolf Fault*	-: 1300	60	7.5	Separating fundamentally recent quaternary fresh basin deposits, vs Mesozoic granite rocks.	*PG&E*	*Gas*	864	*Steel (unknown grade)*	*250*	*400*	1.3	-	-	1.5	Beam Buckling	(Denis, R. 2000)
1968	Meckering Earthquake	Strike-Slip	Meckering Fault	1500: 2000	40	6.9	Precambrian Shield	Goldfields (above g.)	Water	760	Concrete Line Steel Conduits	-	-	2.5	-	-	3.3	Telescoping	(Gordon et al., 1980)
1968	Meckering Aftershock (Oct)	Strike-Slip	Meckering Fault	-	-	3.8	Precambrian Shield	Goldfields (above g.)	Water	760	Concrete Line Steel Conduits	-	-	-	-	-	-	Telescoping	(Gordon et al., 1980)
1971	San Fernando	Thrust	Sylmar Fault Segment	2000: -	19	6.6	Alluvial sand and gravel	Line 115	Gas	400	Steel (unknown grade)	*250*	*400*	2.36	50	2.5	5.9	Local Buckling (wrinkling)	(Southern California Gas Company, 1973)
1987	Edgecumbe	Normal Series of 7 faults	Edge-combe. Await	1000-1500	Max. Seg. 7km	6.3	Z<350mm=Alluvial Plains Ground bellow 14m, marine.	-	*Gas*	100	API-5L Steel	448	531	*1.8*	-	-	18	Tension Yield	(Denis, R. 2000)

Earthqu.		Fault Characteristics					Geology of Area	Pipe Characteristics										Reference
1) Year	2) Location	3) Type	4) Name	5) Maximum Displacement H:V (mm)	6) Length (km)	7) Magnitude of Accompanying Earthquake	8) Geology Description	9) Name	10) Nature of Content	11) Diameter (mm)	12) Material & Condition	13) Yield Stress (Mpa)	14) Ultimate Tensile Stress (Mpa)	15) Fault Offset (m)	16) D/t	17) H/D	18) δ/D	19) Type of Failure	
1988	Tennant Creek	2collinear irregular WNW tending scarps & a shorter ENE tending scarp.	N/A	2000	35	6.8	-	*Near Tennant Creek NT*	*Gas*	350	API X-60 Steel	414	417	2.0	-	-	5.7	Compression deformation	(Denis, R. 2000)
1989	Loma Prieta	Reverse-Slip	Cala-veras (San Andreas)		40	6.9	-	Santa Clara Conduit	Water	2515	-	-	-	-	-	-	-	Joint failure	(Schiff et al., 1998)
1989	Loma Prieta	Reverse-Slip	Cala-veras (San Andreas)		40	6.9	-	Water Main (Hollister)	Water	102	Cast Iron	*130*	*200*	-	9.27	-	-	Joint failure	(Schiff et al., 1998)
1989	Loma Prieta	Reverse-Slip	Cala-veras (San Andreas)		40	6.9	-	Hollister Water Main	Water	102	Asbestos Cement	-	-	-	9.27	-	-	Joint failure	(Schiff et al., 1998)
1999	Chi-Chi Taiwan	Reverse-Slip	Chelung-pu Fault	2000: 10000	80	7.6	Same soil conditions on both sides.	Shigang	Water	2000	Steel	*250*	*400*	10.2	-	-	5.1	Local Buckling	(Schiff et al., 1998)
1999	Turkey Earthquake-August	Right-Lat strike-slip faults	North Anatolian-Sapanca Segment	3000	110	7.8	Soil on one side softer than the other.	Thames Water	Water	2200	Steel	*250*	*400*	3.0	122.22	1.39	1.36	Wrinkling pipe	(Da Ha et al., 2008)
1999	Turkey Earthquake-August	Right-Lat strike-slip faults	North Anatolian-Sapanca Segment	3000	110	8.8	-	Adapazari	Water	700	Asbestos Cement	-	-	3.0	-	-	4.29	Brittle Fracture	(Earthquake Spectra, 2000)
2001	Kokoxili	Strike-Slip with Reverse Slip			450	8.1	-	Oinghai-Xinjiang Border	Oil	170	Steel	-	-	3.6	20	-	21.17	Z Shape buckling deformation	(Guo et al., 2004)

1

APPENDIX B

Figure B-1 shows the deflection of a pipeline crossing strike-slip fault. Let us consider a small segment of the pipe at a distance x from the point A. Thickness of the segment is equal to dx. Axial, shear forces and bending moments developing in the pipe segment and lateral soil forces and axial skin friction between the pipe segment and soil are demonstrated in Figure B-2.

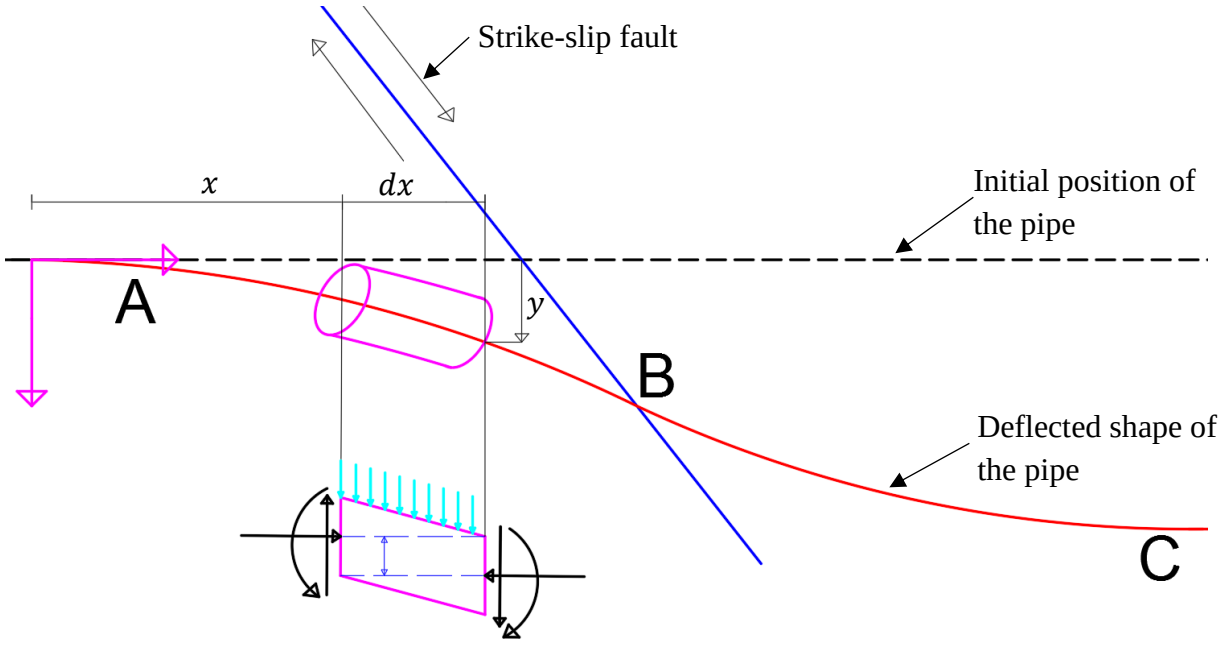

Figure B-1. The deflection of a pipeline crossing strike-slip fault

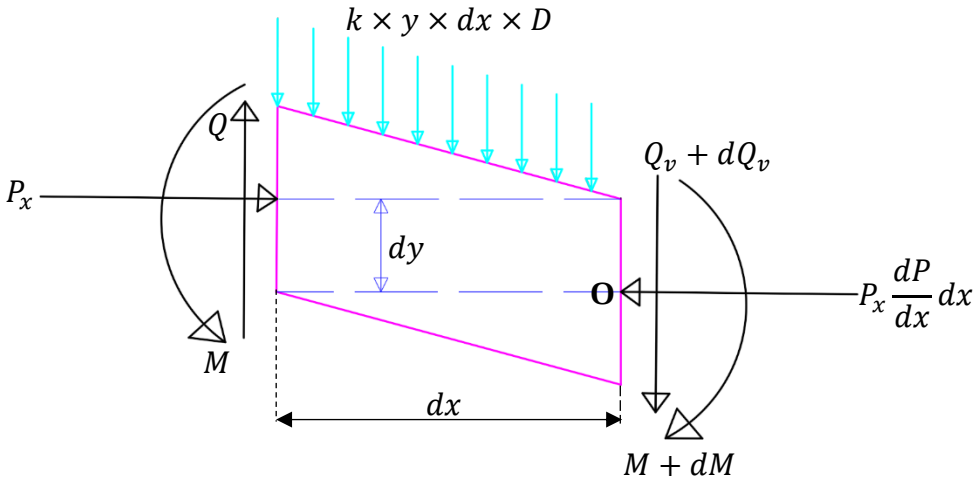

Figure B-2. Stability of the pipe segment

When taking moment about point O, we get:

$$dM + P_x \times dy + Q \times dx - k \times y \times D \times \frac{dx^2}{2} = 0 \qquad (B-1)$$

where k is the modulus of subgrade reaction and D is width of the pipe.

Ignoring $(dx)^2$ term, we get:

$$dM + P_x \times dy + Q \times dx = 0 \qquad (B-2)$$

Differentiating with x,

$$\frac{dM}{dx} + P_x \times \frac{dy}{dx} + Q = 0 \qquad (B-3)$$

Axial force (P_x) can be written as:

$$P_x = P - \int_0^x f(x)dx \qquad (B-4)$$

where $f(x)$ is the friction per unit length and P is external axial load on the pipeline at Point A. In this particular example, P is equal to zero.

By using moment-curvature relationship, bending moment (M) can be stated as:

$$M = EI\frac{d^2y}{dx^2} \qquad (B-5)$$

The change in shear force can be expressed as follow:

$$\frac{dQ}{dx} = +K(x) \times y \qquad (B-6)$$

Substituting equations B-4 and B-6 into equation B-3, we get:

$$EI\frac{d^3y}{dx^3} + \left(-\int_0^x f(x)dx\right)\frac{dy}{dx} + Q = 0 \qquad (B-7)$$

Differentiating equation 8 with x gives:

$$EI\frac{d^4y}{dx^4} + \left(-\int_0^x f(x)dx\right)\frac{d^2y}{dx^2} - f(x)\frac{dy}{dx} + k \times y = 0 \qquad (B-8)$$

Equation B-8 is based on Winkler type beam with effects of axial soil pipe friction. In this equation, tensile behaviour of the soil is neglected.